Title: Climate-induced interannual variability and projected change of two harmful algal bloom taxa in Chesapeake Bay, USA

Authors: Ming Li, Wenfei Ni, Fan Zhang, Patricia M. Glibert and Chih-Hsien (Michelle) Lin

Affiliation: University of Maryland Center for Environmental Science, Horn Point Laboratory, PO Box 775, Cambridge, Maryland 21613, U.S.A.

Submitted to *Science of The Total Environment*

*Correspondence to: Ming Li, University of Maryland Center for Environmental Science, Horn Point Laboratory, 2020 Horn Point Road, Cambridge, MD 21613. Email: mingli@umces.edu.

Abstract

Retrospective analysis of water quality monitoring data reveals strong interannual shifts in the spatial distribution of two harmful algal species (*Prorocentrum minimum* and *Karlodinium veneficum*) in eutrophic Chesapeake Bay. A habitat model, based on the temperature and salinity tolerance of the two species as well as their nutrient preferences, provides a good interpretation for the observed seasonal progression and spatial distribution of these taxa. It also points to climate-induced variability in the hydrological forcing as a mechanism driving the interannual shifts in the algal distributions: both *P. minimum* and *K. veneficum* shift downstream during wetter years but upstream during dry years. Climate downscaling simulations using the habitat model show upstream shifts of the two species in the estuary and longer blooming seasons by the mid-21st century. Salt intrusion due to sea level rise will raise salinity in the estuary and cause these HAB species to migrate upstream, but increasing winter-spring flows may also drive favorable salinity habitat downstream. Warming leads to longer growing seasons of *P. minimum* and *K. veneficum* but may suppress bloom habitat during their respective peak bloom periods.

Keywords: harmful algal blooms; interannual variability; climate change; habitat model; eutrophication; estuary

1 Introduction

Harmful algal blooms (HABs) are escalating worldwide, recognized to be significantly associated with human-induced nutrient pollution as well as global climate change (Anderson et al., 2002; Glibert et al., 2005a, b; Heisler et al., 2008; Hallegraeff, 2010; Fu et al., 2012; Wells et al., 2015; Glibert and Burford, 2017; Glibert 2020). There is little doubt that there are now more HABs, more often, in new and different places, in both fresh and marine waters, often lasting longer, affecting ecosystem and human health with a range of toxicities (Anderson, 1989; Hallegraeff, 1993; Smayda, 2002; Glibert and Burkholder, 2018; Glibert, 2020). There is also little doubt that climate change is impacting species distributions in complex ways, from warming of waters, to altered stratification and changing precipitation patterns (e.g., Paerl and Huisman, 2008; Wells et al., 2015; Glibert, 2020). These changes can act both synergistically and antagonistically with increasing eutrophication trends. For example, while in some regions, increased precipitation, including episodic storm events, increases freshwater flow and the magnitude of nutrient delivery from runoff, increases in drought in other regions may reduce land-based nutrient delivery. Estuaries are particularly susceptible to such fluctuations. Chesapeake Bay, the largest estuary in the U.S., provides an excellent system to investigate the potential impacts of climate change and climate variability on HAB abundance and distribution.

Among the HABs with worldwide, and expanding, global distributions are the planktonic *Prorocentrum* and *Karlodinium* species (Heil et al., 2014; Glibert et al. 2008, 2012; and references therein). In Chesapeake Bay, *K. veneficum* and *P. minimum* (= *P. cordatum*, but note original name maintained here for consistency with data base entries) are among the most common HAB dinoflagellates in the mid to upper reaches of the estuary (Tango et al., 2005; J Li

et al., 2015). Planktonic *Prorocentrum* species are among the most commonly recognized harmful algae that are increasing in frequency, duration, and magnitude globally (Heil et al., 2005; Glibert et al., 2008; 2012); as of 2003, at least 56 species within the genus *Prorocentrum* were known to populate estuarine and marine waters (Gomez, 2005) and of these, at least six species have been shown to form high biomass blooms (Glibert et al., 2012 and references therein). The global expansion of the best-studied pelagic *Prorocentrum* species, *P. minimum*, suggests that this species is spreading in concert with eutrophication (Heil et al., 2005; Glibert et al., 2008; 2012). There are numerous descriptions of this species proliferating in waters influenced by freshwater inputs, especially freshwaters laden with organic forms of nutrients (e.g., Silva, 1985; Granéli et al., 1985, 1989; Stonik, 1995; Grzebyk and Berland, 1996; Glibert et al., 2001; Heil et al., 2005). Numerous records suggest that *Prorocentrum* sp. has flourished in the estuaries of the southeastern U.S. as these systems have become increasingly eutrophic (Glibert et al., 2012 and references therein). In Chesapeake Bay, the dynamics of its transport and seasonal occurrence are well described (Tyler and Seliger, 1978, 1981; Glibert et al., 2001; Tango et al., 2005) and the number of blooms of this species has increased from ~13 per year in the 1990s to >20 per year in the early 2000s (see J Li et al., 2015 for detailed statistical analysis). Tango et al. (2005) found that *P. minimum* blooms were restricted to certain ranges of salinity and temperature and occurred more frequently in April and May. Blooms of *P. minimum* have been associated with anoxic/hypoxic events, finfish kills, aquaculture shellfish kills and submerged aquatic vegetation losses (Heil et al., 2005). One concern of *P. minimum* blooms in Chesapeake Bay is their potential impact on oyster growth and reproduction. While laboratory results have been mixed, with Brownlee et al. (2005) and Stoecker et al. (2008) finding no negative effects of *P. minimum* on oysters for short exposures, Luckenbach et al. (1993) and

Wikfors and Smolowitz (1995) found high mortality of Chesapeake Bay juvenile oysters exposed for more than 10 days to high bloom densities (10^4 to 10^5 cells mL^{-1}) and negative effects on several life stages of eastern oysters.

Blooms of *K. veneficum* are distributed worldwide in estuaries and coasts from Namibia (Braarud, 1957) to Europe (Bjornland and Tangen, 1979), China (Dai et al., 2014), Australia (Ajani et al., 2001; Adolf et al., 2015) and the U.S. (A Li et al., 2000; Adolf et al., 2008; Hall et al., 2008). *Karlodinium spp*. have been found to be responsible for fish deaths worldwide, and are toxic to oyster embryos, larvae, and juveniles which may be a concern in recovery of the Chesapeake oyster fishery (Glibert et al., 2007; Brownlee et al., 2008; Stoecker et al., 2008). Although much has been documented with respect to spatial and temporal distributions of these taxa in Chesapeake Bay, in terms of temperature, salinity and nutrient conditions (Fan et al., 2003; Glibert et al., 2005a, b; Adolf et al., 2008; J Li et al., 2015; Lin et al., 2018a), much less is known with regard to how their seasonal and spatial dynamics vary with climate.

Chesapeake Bay is not only expected to warm considerably over the coming years (Najjar et al., 2010; Irby et al., 2018; Ni et al., 2019), but nutrients are expected to change, and seasonality is expected to shift. Springs in Chesapeake Bay are expected to become wetter, and it is projected that this will increase nitrogen (N) loads – even in the absence of increases in land-based applications; an increase in N flux down the Susquehanna River (the major tributary of Chesapeake Bay) of 17% by 2030 and 65% by 2095 is expected from flow changes alone (Howarth, 2008; Wagena et al., 2018). Moreover, sea level will rise, leading to stronger salt water intrusion and higher salinity, particularly in the lower reaches of the Bay (Hilton et al.,

2008; Hong and Shen, 2012; Ni et al., 2019). A key question is: how will these changes affect potential habitat for HABs such as *P. minimum* and *K. veneficum* in Chesapeake Bay?

In this paper, habitat models for *P. minimum* and *K. veneficum* in Chesapeake Bay were developed and compared to each other and to long-term monitoring data in hindcast mode for years of varying climatic conditions. Then, using climate downscaling approaches, future projections for the mid-21st century were developed. The habitat approach was based on known growth conditions in terms of temperature, salinity and nutrient composition embedded in a spatially explicit biogeochemical model. As such, it provides a relatively simple but insightful method to explore future changes and to aid in the management of these harmful events. The approach taken herein is similar to that applied by Glibert et al. (2014) in developing habitat models for *Prorocentrum* and *Karenia* and climate change projections for the Northwest European Shelf-Baltic Sea and Northeast and Southeast Asia. However, the work herein focuses on two estuarine HABs species in a eutrophic estuary that is expected to be impacted by rapid regional climate change such as faster warming and higher relative sea level rise (Hilton et al., 2008; Najjar et al., 2010; Ding and Elmore, 2015). The habitat models herein for *P. minimum* and *K. veneficum* also differ from the ecological habitat forecasting models developed by Brown et al. (2013). They developed a general logistic regression model of *P. minimum* and an Artificial Neural Network of *K. veneficum*. They then coupled these statistical models to an operational hydrodynamic-biogeochemical model to make daily nowcasts and three-day forecasts for HAB species, with a focus on weather-related events. In contrast, the habitat models developed in this study are directed at understanding long-term changes in HABs and the impacts of climate change and climate variability. The habitat models are used to interpret the observed interannual

variability of *P. minimum* and *K. veneficum* distributions in recent years and to project how climate change will affect the two species in the mid-21st century.

2 Methods

2.1 Data

Phytoplankton abundance, including cell abundance of the targeted HAB species, was acquired from the Chesapeake Bay Program (CBP) (http://www.chesapeakebay.net). The CBP has conducted routine sampling at a number of monitoring stations throughout Chesapeake Bay and its tributaries since the early 1990s. While blooms are not restricted to near-surface waters, the most comprehensive data are available from this depth. Phytoplankton data are reported from samples that had been preserved with acid Lugol's, and were subsequently counted by conventional light microscopy techniques. Details of the enumeration protocols are provided by the Chesapeake Bay Program (2012).

Data on cell abundance of *P. minimum* and *K. veneficum* were mainly available from biweekly sampling in April, May, July, and August, and monthly sampling in March, June, September, October, and December each year. The data analyzed here encompassed only the period from 2002 – 2011 because prior to 2002 the presence of *K. veneficum* was variably reported with different names and was difficult to identify with certainty in the database (Bergholtz et al., 2006). Frequency of sampling and enumeration has declined since 2011, thus making the window from 2002-2011 the most complete data set for a comparative study of *P. minimum* and *K. veneficum*.

The Susquehanna River provides most of the freshwater to the upper and middle parts of Chesapeake Bay. Flows at the Susquehanna River were measured at a station near the Conowingo Dam and downloaded from the U.S. Geological Survey website (http://waterdata.usgs.gov; station 01578310).

2.2 Habitat model

The habitat models for *P. minimum* and *K. veneficum* are built upon a coupled hydrodynamic-biogeochemical modeling system that was recently developed for Chesapeake Bay (Testa et al., 2014; M Li et al., 2016; Testa et al., 2017; Shen et al., 2019). The hydrodynamic model is based on the Regional Ocean Modeling System (ROMS, Shchepetkin and McWilliams, 2005; Haidvogel et al., 2008), and has 82×122 grid points (~1 km resolution) in the horizontal direction and 20 layers in the vertical direction (M Li et al., 2005; Xie and Li, 2018; Fig. S1). ROMS is forced by river flows at major tributaries, by wind stress and heat fluxes at the sea surface, and by tidal and subtidal sea levels and climatology of temperature and salinity at the open boundary. ROMS was initialized on 1 January 2000 and run continuously until 31 December 2011. Results from the spin-up period of 2000 and 2001 were not analyzed. ROMS outputs were saved at hourly intervals and then used to drive the biogeochemical model in an offline mode. The ROMS hydrodynamic model has been validated against an extensive set of observational data, including water levels, temperature, salinity and currents (e.g. M Li et al., 2005; Zhong and Li, 2006; M Li et al., 2006; Xie and Li, 2018; Xie et al., 2018).

The biogeochemical model is based on the Row-Column Aesop (RCA) model (Isleib et al., 2007; Fig. S1). RCA simulates two generic phytoplankton groups (a winter and a summer

community), particulate and dissolved forms of carbon and nutrients, and dissolved oxygen in the water column, and is coupled to a sediment diagenesis component (Di Toro, 2001). RCA is forced by the loads of particulate and dissolved forms of inorganic and organic nutrients as well as organic carbon from the tributaries (https://www.chesapeakebay.net/). RCA was initialized on 1 January every year using the water-quality data collected in the preceding month. The RCA biogeochemical model has been validated against an extensive set of water quality data in Chesapeake Bay (Testa et al., 2014; M Li et al., 2016; Irby et al., 2016; Testa et al., 2017).

Both *P. minimum* and *K. veneficum* have been well characterized physiologically, and based on literature from Chesapeake Bay and elsewhere (e.g., Heil et al., 2005; Tango et al., 2005; Glibert et al., 2012; J Li et al., 2015; Lin et al., 2018a), an envelope of physical and chemical parameters which produced favorable habitat conditions for growth was defined for each taxa (Table 1). The chemical niche is based on the observed preference of these species for regenerated N (i.e., chemically reduced forms) over new N (i.e, oxidized forms; A Li et al., 1999; Fan et al., 2003; Place et al., 2012; Glibert et al., 2014). In that our goal was to define potential habitat rather than to model biomass accumulation, a ratio approach was used rather than defining absolute nutrient concentrations and their relationships to growth rate (c.f., Glibert et al., 2014). The outcomes of the model projections are spatial and temporal estimates of the space and time over which specific habitat parameters–that are thought to be suitable for HAB growth–occur individually or collectively. Although there is no one-to-one correspondence between the habitat suitability and cell density, habitat models have been widely used to examine how changing environmental conditions affect marine species (e.g. Niklitschek and Secor, 2005;

215 Schlenger et al., 2013; Glibert et al., 2014; Smith et al., 2018), in the same way as done in this
216 paper.
217
218 *2.3 Hindcasting and climate downscaling projections*
219 To understand observed interannual variability in the biomass and spatial distribution of
220 *P. minimum* and *K. veneficum*, hindcast simulations of habitat suitability were conducted and
221 compared to the 10-year period (2002-2011) for which the monitoring data on the two species
222 were most complete. To project how climate change might affect the species in the future, the
223 ROMS-RCA model was forced with downscaled climate projections from the Regional Climate
224 Models (RCMs) in the North American Regional Climate Change Assessment Program
225 (NARCCAP) (Mearns et al., 2009) for the 10-year period 2052-2061, 50 years after the 2002-
226 2011 monitoring record period. RCMs were used to prescribe the air-sea momentum and heat
227 fluxes. RCMs include basic land-surface schemes that interact with the atmosphere to generate
228 surface runoff but do not include river routing models that can simulate streamflow. In this study
229 the delta method was used to generate future changes in river flows by using the integrated
230 surface runoff over the watershed (Teutschbein and Seibert, 2012). General Circulation Models
231 (GCMs) projections for the Northwest Atlantic Ocean were used to prescribe changes in the
232 offshore boundary condition for ROMS-RCA. Of particular interest is how salinity may change
233 due to sea level rise. The relative sea level rise was set to be the sum of the GCMs sea level
234 projection for the region and local sea level rise due to land subsidence (Zervas, 2009), following
235 Lee et al. (2017). To correct the biases in the NARCCAP meteorological outputs, the empirical
236 quantile mapping method was applied, using the historical data from the North American
237 Regional Reanalysis (NARR) as the observational reference (Mesinger et al., 2006;

238 Gudmundsson et al., 2012). Ni et al. (2019) used this downscaling approach to project future
239 changes in hypoxia in Chesapeake Bay.
240
241 NARCCAP consists of 12 RCM-GCM combinations (Mearns et al., 2009), and 3 of these
242 were selected for the climate downscaling simulations, based on NARCCAP data availability in
243 the study area and the range of predicted changes in streamflow and air temperature. The
244 selected RCM-GCM models included RCM3-gfdl - the Regional Climate Model version 3
245 (RCM3; Pal et al., 2007) driven by the Geophysical Fluid Dynamics Laboratory model (gfdl;
246 Delworth et al., 2006); HRM3-hadcm3 - the Hadley Regional Climate Model (HRM3, Jones et
247 al., 2004) driven by the Hadley Centre Coupled Model version 3 (hadcm3, Gordon et al., 2000);
248 and WRFG-cgcm3 - the Weather Research and Forecasting Grell model (WRFG; Skamarock et
249 al., 2005) driven by the Third Generation Coupled Global Climate Model (cgcm3; Flato et al.,
250 2005).
251
252 *2.4 Analysis of habitat model results*

253 Using the habitat model, the fraction of a year, T_f, when physical conditions and/or
254 chemical conditions produce favorable habitats for *P. minimum* or *K. veneficum* anywhere in the
255 estuary was calculated. An area with larger T_f implies that habitat conditions are favorable for the
256 bloom development. The fraction of the surface area, A_f, in the Bay that produce favorable
257 conditions at any time in the year for the respective blooms was also calculated. If A_f is high in a
258 particular month, it implies that more areas in the estuary produce favorable habitat condition for
259 the HABs species. Both T_f and A_f are non-dimensional.
260

To provide a quantitative comparison between the observed cell distribution and predicted favorable habitat area, the center of cell mass was calculated using the cell concentration measurements at the monitoring stations:

$$\overline{Y}_{obs} = \frac{\oiint yCdydx}{\oiint Cdydx} \quad (1)$$

where C is the annual average of cell concentration of either *P. minimum* or *K. veneficum* in the surface water, x is the coordinate in the longitudinal direction, y is the coordinate in the latitudinal direction, and $\overline{Y}_{obs}$ is the observed center of mass for *P. minimum* or *K. veneficum*. Similarly, T_f was used to calculate the center of mass $\overline{Y}_{mod}$ expected from the habitat model:

$$\overline{Y}_{mod} = \frac{\oiint yT_f dydx}{\oiint T_f dydx} \quad (2)$$

where the integrals in Eq. (2) cover all model grid points in the estuary.

3 Results

3.1 Climatological mean HABs distribution

When averaged over the 10-year period representing current conditions, the cell density of *P. minimum* and *K. veneficum* derived from the Chesapeake Bay monitoring program shows distinctive spatial patterns (Figs. 1a, 1b). Although *P. minimum* has low cell density ($<10^6$ cells L^{-1}) in the lower part of the estuary (south of 38 ^{o}N latitude), high cell concentrations ($>10^7$ cells L^{-1}) are found in the middle part of the estuary (between 38 and 39.3 ^{o}N), with the highest cell density of *P. minimum* near 38.5 ^{o}N (Fig. 1a). In comparison, *K. veneficum* cells are generally absent south of 38 ^{o}N latitude. High concentrations of *K. veneficum* (>5 x 10^6 cells L^{-1}) are found

between 38.5 and 39.3 ^{o}N, further north than *P. minimum* (Fig. 1b). The highest cell density of *K. veneficum* is found in the northern limit at 39.3 ^{o}N.

The seasonal progression of *P. minimum* and *K. veneficum* blooms are also strikingly different (Figs. 2a, b). *P. minimum* reaches its peak cell density during the spring months of April and May, but a small second peak appears in the averaged data in December (Fig. 2a). Cell concentrations of *P. minimum* are low during the summer. In contrast, the *K. veneficum* growing season spans from April to September, with blooms peaking in June and July (Fig. 2b). Monthly averaged concentrations of both HAB species show a wide range over the 10-year period, particularly during their respective blooming seasons (May for *P. minimum* and June and July for *K. veneficum*).

The T_f values calculated using the habitat model based on the physical niche compared well with the observed spatial distribution of the cell concentrations (Fig. 1). For *P. minimum*, large values of T_f were found in the region between 38.2 and 39.1 ^{o}N, which was broadly consistent with the region of observed high *P. minimum* cell density (compare Figs. 1a, 1c). High values of T_f for *K. veneficum* were found in the region between 38.6 and 39.3 ^{o}N, which was co-located with the region of observed high *K. veneficum* cell density (compare Figs 1b, 1d).

While the T_f estimate is not the same as bloom duration because actual bloom development also depends on other factors such as light and grazing, the A_f values calculated from the physical habitat model provide a reasonable interpretation for the observed timing of the *P. minimum* and *K. veneficum* blooms (Figs. 2c, 2d). About 25% of the area in Chesapeake

Bay were favorable for the *P. minimum* blooms in April and May (Fig. 2c), which corresponds to the two months that had the highest cell density observed at the monitoring stations (compare Fig. 2c, Fig. 2a). The habitat model suggested a second peak in A_f in the fall. This potential growth niche was generally not realized in the cell density, although the observed *P. minimum* cell concentration indicated a small peak in December (Fig. 2a) and previous observations have shown a fall *P. minimum* bloom in some years (e.g. Tango et al., 2005; J Li et al., 2015). The fraction of the Bay's surface area that produced favorable physical habitats for *K. veneficum* blooms had a closer match with the observed cell density, with the highest values of A_f in June and July (compare Figs. 2b, 2d). The model-predicted bloom area was consistently large when high *K. veneficum* concentration was observed, spanning from May to September.

Compared with the physical habitat constraints (temperature and salinity ranges) of *P. minimum* and *K. veneficum* growth, defining potential habitat based on the chemical niche (nutrient proportions) revealed a suitable habitat south of ~38 ^{o}N, but less suitable habitat north of it and no distinction spatially between the two species (Figs. 3a,c). The Susquehanna River, in the northern limit of Chesapeake Bay, delivers most of the riverine N in the form of NO_3^- to the upper and middle parts of the Bay. Concentrations of NO_3^- remain much higher than the chemically-reduced N form, NH_4^+, in those regions until it is exhausted during the summer. On the other hand, most of the N in the lower Bay is NH_4^+. The chemical niche restricted the habitat in the upper Bay, but was not as restrictive as the physical criteria elsewhere. When considering the physical and chemical criteria together, the average fraction of the year in the complete habitat model showed a pattern similar to the model based on the physical criteria only (Figs. 3b, d).

328

329 *3.2 Interannual shifts in the spatial distribution of P. minimum and K. veneficum*

330 Between 2002 and 2011, there were large interannual variations in the hydrological
331 forcing of Chesapeake Bay. The Susquehanna River flow was high during 2003-2005 and 2010-
332 2011 (wet years) but low during 2006-2009 (dry years) (Fig. 4). Total N (TN) loading and total P
333 (TP) loading co-varied but did not display any long-term trends over this 10-year period.

334

335 Annually-averaged cell concentrations of *P. minimum* observed at the monitoring stations
336 varied considerably between 2002 and 2011 (Fig. 5). During 2003, 2005, and 2011, years with
337 high river flows, high *P. minimum* concentrations were found around 38.5 ^{o}N. In contrast, high
338 cell densities were found around 39-39.2 ^{o}N, much further north, during the dry years of 2007,
339 2008, and 2009. However, there were exceptions. No blooms were observed during 2004, which
340 was a wet year, 2002, which was a year with average flows, and 2010, which was a moderately
341 wet year. Since *P. minimum* blooms mostly occurred in April and May, the timing of high river
342 flows differed in these years. In 2004, high flows were observed during summer; in 2002, the
343 spring flows were delayed relative to average and the summer months had below average flows;
344 and in 2010, although spring flows were high, the flows were earlier than average (Fig. S2).
345 Also, in 2006, another dry year, no large blooms were observed but the cell density was
346 relatively uniform between 38 and 39.2 ^{o}N. Nevertheless, there were striking interannual
347 differences in the spatial distribution of *P. minimum*: it shifted southward (downstream) during
348 the wet years and northward (upstream) during the dry years. Thus, this simple model based on
349 physical habitat could explain a significant part of the observed interannual variability in the *P.*
350 *minimum* distribution. No significant differences were found in the timing of *P. minimum* blooms

during the 10 years: the peak bloom always occurred during May (Fig. S3). Unlike the river flows and salinity in the estuary, temperature had a well-defined seasonal cycle and did not display significant interannual variability (Fig. S4).

Similar interannual shifts in the spatial distribution of *K. veneficum* were found as those of *P. minimum* (Fig. 6). High cell densities were found in the southern region (~38.6 ^{o}N) during the wet years of 2003, 2005, and 2010, but shifted to the northern region (39-39.2 ^{o}N) during the dry years of 2006, 2007, 2008, and 2009. No significant blooms were observed during 2002 (average runoff), 2004 (wet), and 2011 (wet). As was the case for *Prorocentrum* blooms, the timing of the wet season varied, even for those years that had above average flows. While 2002 was an above average flow year, the summer had flows that were below average (Fig. S2). In the cases of 2004 and 2011, the summer flows were well above average. The monthly averaged cell concentration of *K. veneficum* did not show systematic differences between the wet and dry periods (Fig. S5). There were large scatters, mostly due to small sample sizes. It may be inferred that *K. veneficum* blooms lasted longer during the dry years (2007, 2008, and 2009) while they were of a shorter duration during the wet years (2003, 2004, 2005, 2011).

The habitat model based on the physical criteria provided a reasonable interpretation for the observed interannual shifts of *P. minimum* and *K. veneficum* blooms between 2002 and 2011 (Figs. 5, 6). Areas with a high probability of *P. minimum* blooms, as represented by a high fraction of year with favorable physical habitat, shifted towards the mid and lower Bay during the wet years of 2003-2004 and 2010-2011 but shifted towards the upper Bay during the dry years of 2007-2009 (Fig. 5). The counter example is the dry year of 2006 when the habitat model

still predicted *P. minimum* bloom occurrences in the mid Bay. There was, in general, good correspondence between the region of high cell abundance and the area with the favorable physical habitat. The shifting of the suitable habitat area with river flows was consistent with the shifts of the *P. minimum* blooms between the years. The habitat model also provided a good interpretation of the interannual shifts of *K. veneficum* distribution over the 10-year period (Fig. 6). The suitable habitat area moved downstream during the wet years of 2003, 2004, and 2011. In contrast, it was confined to the upper Bay during the four dry years of 2006-2009. Two exceptions were the wet years of 2005 and 2010 when the habitat model predicted favorable habitats in the upper Bay.

To provide a quantitative comparison between the observed cell distribution and the predicted favorable habitat area, the centers of mass $\overline{Y}_{obs}$ and $\overline{Y}_{mod}$ were calculated and plotted against the annual mean flow $\bar{Q}$ from the Susquehanna River. The relationship between $\overline{Y}_{obs}$ and $\bar{Q}$ for *P. minimum* showed wide scatters (Fig. 7a), but the center of mass of *P. minimum* generally shifted southward with increasing river flow. The least square fit of a linear regression showed a downward trend, although the coefficient of determination $r^2 = 0.11$ is low and the *p*-value of 0.35 is high. Removing the two outlier years (2010 and 2011) improves the regression, with $r^2 = 0.44$ and $p = 0.07$. A stronger correlation between $\overline{Y}_{obs}$ and the river flow appeared in the relationship with *K. veneficum*, with $r^2 = 0.45$ and $p = 0.03$ as well as a steeper slope (i.e. stronger dependence on the river flow) (Fig. 7c). Moreover, the center of mass for *K. veneficum* (between 38.4 and 39.1 ^{o}N) lay further north than *P. minimum* (between 37.9 and 38.4 ^{o}N). The calculated $\overline{Y}_{mod}$ for both *P. minimum* and *K. veneficum* decreases with the river flow, with $r^2 = 0.69$ and 0.83 and *p*-values of 0.003 and 0.0002, respectively (Figs. 7b, 7d). The

predicted center of mass was in good agreement with the observed one for *K. veneficum*, but $\overline{Y}_{mod}$ lay further north than $\overline{Y}_{obs}$ for *P. minimum*, indicating a possible bias in the habitat model. For comparison, a linear fit to the observed cell distribution using the same slope as in the habitat model was applied (dashed lines in Figs. 7a, 7c). It should be noted that $\overline{Y}_{obs}$ was calculated from cell concentration measurements at a few monitoring stations whereas $\overline{Y}_{mod}$ was calculated from at all model grid points in the estuary. This mismatch in the spatial resolution between the observations and model was likely a source for the model-data discrepancy, such that it was difficult to make a precise comparison between $\overline{Y}_{obs}$ and $\overline{Y}_{mod}$.

3.3 Climate downscaling projections for the mid-21st century

To project how climate change might affect *P. minimum* and *K. veneficum* blooms in the mid-21st century, ROMS-RCA was forced by the downscaled projections from the three RCM models included in the NARCCAP ensemble: WRFG_cgcm3, RCM3_gfdl and HRM3_hadcm3. All three models predict substantial increases in the annual mean air temperature between 2002-2011 and 2052-2061 (Fig. 8). These models also predict increases in the Susquehanna River flow in winter but slight reductions in summer. Nevertheless, there are inter-model differences, reflecting the uncertainty in the RCMs projections for the future climate. The WRFG_cgcm3 model projects higher temperature increases (about 1.7 ^{o}C) with weaker seasonal variations. It also predicts increases in the river flow in winter and spring, small reduction in summer and large increases in the fall. The RCM3_gfdl model predicts moderate warming (about 1.3 ^{o}C) with strong seasonal variations. It projects increases in winter discharge but decreases in river flow in the other three seasons. The HRM3_hadcm3 model predicts relatively moderate increases in temperature (about 1.4 ^{o}C) but with strong seasonal variations, and large increases in winter river

flows with small changes of either sign during other seasons. The projected relative sea level rise for the mid-21st century is 0.45 m in WRFG_cgcm3, 0.43 m in RCM3_gfdl, and 0.31 m in HRM3_hadcm3.

The habitat model was used to calculate changes in the suitable habitat for *P. minimum* and *K. veneficum* blooms between 2002-2011 and 2052-2061 ($\Delta T_f = T_{f2052:2061} - T_{f2002:2011}$), based on the physical criteria only. With RCM_gfdl as an example, substantial changes in the spatial bloom habitat were found (Fig. 9). For *P. minimum*, the bloom probability is projected to increase in the region around 39.1-39.4 ^{o}N in the upper Bay but to decrease in the region south of ~39 ^{o}N. A similar upstream shift is projected for the *K. veneficum* blooms for 2052-2061. The upper Bay region of 39.1-39.4 ^{o}N is thus likely to see large increases in *K. veneficum* blooms, whereas suitable bloom habitat elsewhere will be reduced. However, it must be pointed out that the northernmost region of Chesapeake Bay north of 39.4 ^{o}N will only see a modest increase in the suitable habitat for both *P. minimum* and *K. veneficum* blooms (Fig. 9).

The effect of temporal changes in future habitat appears to be largely a function of temperature, a direct consequence of warming, as shown by all 3 model scenarios (Fig. 10). The WRFG_cgcm3 climate model projects the largest temperature increase and relatively uniform increases over a year. Both the spring and fall *P. minimum* blooms shift away from the hot summer: the spring bloom shifts earlier while the fall bloom shifts later in the year (Fig. 10a). Higher summer temperature moves some days in July and August out of the preferred temperature range for *K. veneficum* blooms, but extends the bloom season earlier to May and later to October (Fig. 10d). While the summer occurrences of *K. veneficum* blooms will likely be

443 reduced under this scenario, more *K. veneficum* blooms will occur in spring and fall. Similar
444 seasonal shifts in *P. minimum* and *K. veneficum* blooms are projected in the two other RCMs:
445 RCM3_gfdl and HRM3_hadcm3 (Figs. 10b, c, e, f). The spring *P. minimum* bloom may shift
446 early from May to April, while the fall bloom may shift later. *K. veneficum* will likely have a
447 long blooming season from May to October, but its peak density may be reduced during the hot
448 summer months of July and August.
449
450 Spatial changes in future habitat of the blooms studied here, ΔT_f, appear to be driven in
451 large part due to changes in salinity (Figs 11, 12). In the model run driven by RCM3_gfdl, the
452 favorable habitat area for *P. minimum* retreats from its southern limit, as sea level rise causes
453 stronger salt intrusion and higher salinity water in the lower Bay (Fig. 11). The northern limit of
454 the favorable habitat area also shifts northward but fails to reach the northern-most region of the
455 upper Bay. There are large uncertainties in the projection of precipitation and river runoff among
456 the climate models (Fig. 8), thereby resulting in different projections for the favorable salinity
457 habitat (Fig. 11). HRM3_hadcm3 projects large increases in winter runoff but modest sea level
458 rise. This significantly lowers surface salinity during spring and shifts the favorable salinity
459 habitat for *P. minimum* downstream. In the model run driven by WRFG_cgcm3, the effects of
460 sea level rise and stronger river flows oppose each other, leading to small changes in the salinity
461 habitat for *P. minimum*. For *K. veneficum*, with its lower salinity tolerance range, an upstream
462 shift of the favorable habitat area is predicted in two models: WRFG_cgcm3 and RCM3_gfdl
463 (Fig. 12). During its peak blooming season in the summer, the effects of river flows on salinity
464 are weaker and salt intrusion due to sea level rise likely drive the upstream shift of its more
465 favorable salinity habitat. Nevertheless, the habitat changes are quite different in the model run

466 driven by HRM3_hadcm3 because of its projected modest sea level rise and large river flow
467 increases.
468

469 **4 Discussion and Conclusion**

470 Herein, a relatively simple habitat model was built for two common Chesapeake Bay taxa
471 using physical criteria and nutrient ratios. This model demonstrates that physical and chemical
472 factors regulate the temporal and spatial habitat of these target taxa and explain the observed
473 interannual shifts of the HABs locations between wet and dry years. In this study, climate-
474 induced changes in riverine nutrient loading come from projected changes in precipitation and
475 associated flow-derived runoff. Potential impacts of climate-induced changes in watershed
476 denitrification and riverine nutrient concentration (Howarth et al., 2006; Schaefer et al., 2007)
477 were not considered. Our habitat model does not describe growth of the species per se. These
478 taxa are both recognized to display mixotrophic feeding (e.g., Stoecker et al. 1997, A Li et al.
479 2000, Adolf et al. 2008, Johnson 2014, Lin et al. 2018b) and therefore food availability could be
480 considered to be important in defining habitat. A separate mechanistic modeling effort is
481 currently underway to incorporate the mixotrophic model of Flynn and Mitra (2009) into ROMS-
482 RCA for these HAB taxa (Lin et al., 2018b). In this paper, the simplest model possible was
483 purposely chosen to determine how much of the observed variability in the two HABs species
484 could be explained by simple factors. Regardless of its simplicity, the habitat niche as identified
485 here explained the climatological mean locations of the blooms, the seasonal timing of the
486 blooms, and the interannual variability in the bloom locations (Figs. 1, 2, 5, 6, 7). Without any
487 consideration of top-down factors or grazing relationships, the habitat model provides a
488 reasonable explanation for the measured abundances. Moreover, insight can be gained from

mismatches as well as matches; for example, the unrealized fall habitat of *P. minimum*. Lack of actualized blooms during this time of year may be due to higher grazing pressure at that time, and further field data and modeling may reveal the factors that increase in importance at that time. It is of note that large fall *P. minimum* blooms have been observed in several recent years.

The models also did not take into account growth rate changes that may be associated with complex interactions of atmospheric increases in CO_2 and temperature (e.g., Finkel et al., 2010; Fu et al., 2012; O'Neil et al., 2012; Boyd and Hutchins, 2012; Wells et al., 2015; Flynn et al., 2015; Sommer et al. 2015; Glibert and Burford, 2017; Glibert and Burkholder, 2018; Glibert 2020 among others). Increasing levels of CO_2 may favor algae that depend on diffusive CO_2 rather than HCO_3^- as their C source or those that that may downregulate their C concentrating mechanisms and therefore reallocate energy to different pathways (Raven et al., 2005; Rost et al., 2006; Beardall et al., 2009). This latter description includes many harmful algal species (Dason et al., 2004), but this is not the case for all HABs. Future iterations of this model will include growth rate changes due to anticipated CO_2 changes, but there is work yet to be done in characterizing these physiological changes. Recent laboratory results suggest that changes in seawater carbonate chemistry due to ocean acidification may adversely affect the growth of *K. veneficum* (Müller et al., 2019).

The ROMS-RCA models are configured over a structured grid (Fig. S1). Although the model domain covers the major tributaries to Chesapeake Bay, it does not have fine resolutions to resolve small-scale processes in small tributaries such as the Patapsco River (see Fig. 1d for its location), a common location for *K. veneficum*. However, the main objective of this paper was to

investigate estuary-wide shifts of the two HABs species due to climate variability/change and to gain an understanding of the driving mechanisms. It is not the goal to provide a precise prediction of specific bloom sites in the future climate. Since the temperature and salinity fields used in our habitat model are mostly determined by air-sea heat fluxes and flows from the major tributaries, they are continuous in space and time in the estuary such that a similar habitat condition is expected in a small tributary adjacent to a main stem area. In other words, if the habitat model predicts high HABs probability in an area in the main stem, the small adjacent tributary is also expected to be prone to the HABs even though this tributary is not well resolved in ROMS. However, the habitat model predictions in some tributaries clearly need to be improved. For example, the habitat model predicts small areas in the Patuxent River and James River to produce favorable habitat condition for *K. veneficum*, but they were not reflected in the cell density measurements (compare Figs. 1b,1d).

It should also be pointed out that the relationship between $\overline{Y}_{obs}$ and the Susquehanna River flow is weaker for *P. minimum* than for *K. veneficum*. Some of these blooms occurred in tributaries which may receive large amounts of urban wastewater discharge, creating eutrophic conditions favorable for the HABs growth (J Li et al., 2015). These factors likely complicate the relationship between the cell density and physical habitat, and may explain the scatters seen in Fig. 7a. A mechanistic HABs model which takes nutrient kinetics into account would be needed to improve these HAB predictions, and is under development.

Despite these model limitations, it was encouraging that a simple habitat model based on the temperature and salinity tolerance ranges alone explained about a significant part of the

observed interannual shifts in the spatial distributions of *P. minimum* and *K. veneficum* blooms. Even with this comparatively simple approach, much insight was obtained into not only how habitat may change, but also the mechanisms driving such changes. Climate forcing is well recognized to be a key driver of interannual variability in phytoplankton biomass in Chesapeake Bay. Miller and Harding (2007) showed that the spring bloom (as measured by Chlorophyll *a*) is larger and occurs farther seaward during wet and warm years than during dry and cool years. Analysis of phytoplankton composition further showed large increases of diatoms, but modest decreases of summer dinoflagellates, in wet years compared to dry years (Adolf et al., 2006; Harding et al., 2015). This work extends such analysis to individual phytoplankton species, *P. minimum* and *K. veneficum*.

The habitat modeling approach taken here is similar to that taken by Glibert et al. (2014) who modeled habitat suitability of comparable taxa, *Prorocentrum* spp. and *Karenia* sp. for the NE European/Batic Sea region, NE Asia and SE Asia. This approach differed from Glibert et al. (2014) in that different physical and biogeochemical underlying models were applied; sea level rise was accounted for; and multiple global climate models were applied in future projections. As in the Glibert et al. (2014) application, future projections are based on climate projections alone and do not account for anthropogenic changes in nutrients that may come from escalating human activities or from nutrient management actions. Glibert et al. (2014) found an expansion in area and/or duration annually conducive to development of *Prorocentrum* and *Karenia* blooms in cold regions such as the Northwest European Shelf-Baltic Sea and Northeast Asia but no expansion (*Prorocentrum* spp.) or contraction (*Karenia* spp.) in the area and duration conducive for blooms in warm regions such as Southeast Asia. Changing temperature was found to be the

dominant driver in Northwest European Shelf-Baltic Sea, a major driver in Northeast Asia, and an important factor in Southeast Asia. In none of these regions was salinity found to be a factor in driving the changes of these two HABs genera. The results herein on favorable habitat (Figs. 11 and 12) differ from the Glibert et al. (2014) finding that warming was the main driver of the HAB changes in coastal oceans. In an estuary like Chesapeake Bay, salinity change drives the shifts in the spatial distribution of the two HABs genera. As shown by Hilton et al. (2008) and Hong and Shen (2012), sea level rise caused stronger salt intrusion into the estuary. Climate change may also lead to large changes in hydrological cycles and river flows, affecting salinity distribution in the estuary (Najjar et al., 2010; Ni et al., 2019). Therefore, it is important to consider climate-driven salinity changes due to sea level rise and changing river flows when projecting future habitat for the HABs in estuarine systems.

In summary, the habitat modeling approach used here has shown that physical and chemical factors are good explanatory variables with respect to the temporal and spatial habitat of *P. minimum* and *K. veneficum* in Chesapeake Bay. The model also explains the climatological mean locations and observed seasonal timing of blooms, and the interannual shifts of the HAB bloom locations between wet and dry years. These models, together with the forthcoming mechanistic models of these target species, provide management tools that may aid in assessment of regional vulnerability to these HABs and how they may change under future conditions.

Acknowledgments:

We thank two reviewers for their careful comments. The authors received support from the National Oceanic and Atmospheric Administration National Centers for Coastal Ocean Science Competitive Research program under award No. NA17NOS4780180. This is contribution

number xxxx of the University of Maryland Center for Environmental Science and number ECOyyy from the NOAA ECOHAB program.

Data availability:

The water quality monitoring data analyzed in this paper can be downloaded from https://doi.org/10.5281/zenodo.3351676. The model outputs can be downloaded from http://doi.org/10.5281/zenodo.3352218 and http://doi.org/10.5281/zenodo.3352248.

References:

Adolf, J. E., Bachvaroff ,T., Place A. R., 2008. Can cryptophyte abundance trigger toxic *Karlodinium veneficum* blooms in eutrophic estuaries? Harmful Algae 8, 119-128.

Adolf, J.E., Yeager, C.L., Miller, W.D., Mallonee, M.E., Harding Jr., L.W. 2006. Environmental forcing of phytoplankton floral composition, biomass, and primary productivity in Chesapeake Bay, USA. Est., Coast. & Shelf Sci. 67, 108-122.

Adolf, J. E., Bachvaroff, T. R., Deeds, J. R., Place A. R. 2015. Ichthyotoxic *Karlodinium veneficum* (Ballantine) J Larsen in the upper Swan River estuary (Western Australia): Ecological conditions leading to a fish kill. Harmful Algae 48, 83-93.

Ajani, P., Hallegraeff, G., Pritchard, T. 2001. Historic overview of algal blooms in marine and estuarine waters of New South Wales, Australia. Proc. Linn. 123, 1-22.

Anderson, D. M. 1989. Toxic algal bloom and red tides: a global perspective. In: Okaichi, T., Anderson, D.M., Nemoto, T. (Eds.), Red tides: biology, environmental science and technology (pp. 11-16). Elsevier.

Anderson, D.A., Glibert, P.M., Burkholder, J.M. 2002. Harmful algal blooms and eutrophication:

Nutrient sources, composition, and consequences. Estuaries 25, 562-584.

Beardall, J., Stojkovic, S., Larsen, S. 2009. Living in a high CO_2 world: impacts of global climate change on marine phytoplankton. Plant Ecol. Divers. 2(2), 191–205.

Bergholtz, T., Daugbjerg, N., Moestrup, Ø., Fernández, T.M. 2006. On the identity of *Karlodinium veneficum* and description of *Karlodinium armiger sp. nov.* (dinophyceae), based on light and electron microscopy, nuclear-encoded LSU rDNA, and pigment composition1. J Phycol. 42, 170-193.

Bjornland, T., Tangen, K. 1979. Pigmentation and morphology of a marine *Gyrodinium* (Dinophyceae) with a major carotenoid different from peridinin and fucoxanthin. J. Phycol. 15, 457-463.

Boyd, P.W., Hutchins, D.A. 2012. Understanding the responses of ocean biota to a complex matrix of cumulative anthropogenic change. Mar. Ecol. Prog. Ser. 470, 125–135.

Braarud, T. 1957. A red water organism from Walvis Bay (*Gymnodinium galatheanum* n. sp.). Galathea Deep Sea Expedition 1, 137-138.

Brown, C.W., Hood, R.R., Long, W., Jacob, J. et al. 2013. Ecological forecasting in Chesapeake Bay: using a mechanistic-empirical modeling approach. J. Mar. Sys. 125, 113-125.

Brownlee, E.F., Sellner, S.G., Sellner, K.G. 2005. *Prorocentrum minimum* blooms: potential impacts on dissolved oxygen and Chesapeake Bay oyster settlement and growth. Harmful algae 4, 593-602.

Brownlee, E.F., Sellner, S.G., Sellner, K.G., Nonogaki, H., Adolf, J.E., Bachvaroff, T.R., Place, A.R. 2008. Response of *Crassostrea virginica* (Gmelin) and *C. ariakensis* (Fujita) to bloom-forcing phytoplankton including ichthyotoxic *Karlodinium veneficum* (Ballantine). J. Shellfish Res. 27, 581-591.

628 Chesapeake Bay Program. 2012. The 2012 user's guide to Chesapeake Bay Program biological
629 monitoring data. EPA 003R 903R 12-002.
630 https://www.chesapeakebay.net/documents/3684/guide2012_final.pdf
631 Dason, J.S., Huertas, I.E., Colman, B. 2004. Source of inorganic carbon for photosynthesis in
632 two marine dinoflagellates. J. Phycol. 40, 285-292.
633 Dai, X., Lu, D., Guan, W., Wang, H., He, P., Xia, P., Yang, H. 2014. Newly recorded
634 *Karlodinium veneficum* dinoflagellate blooms in stratified water of the East China Sea.
635 Deep Sea Res. II 101, 237-243.
636 Delworth, T.L., Broccoli, A.J., Rosati, A., Stouffer, R.J., Balaji, V., Beesley, J.A., et
637 al. 2006. GFDL's CM2 global coupled climate models. Part I: formulation and
638 simulation characteristics. J.f Clim. 19, 643–674.
639 Di Toro, D.M. 2001. Sediment flux modeling. Wiley-Interscience, New York, 624 pp.
640 Ding, H., Elmore, A.J. 2015. Spatio-temporal patterns in water surface temperature from Landsat
641 time series data in the Chesapeake Bay, U.S.A. Remote Sens. Environ. 168,335-348.
642 Fan, C., Glibertm P.M., Alexanderm J., Lomas, M.W. 2003. Characterization of urease activity
643 in three marine phytoplankton species, *Aureococcus anophagefferens*, *Prorocentrum*
644 *minimum*, and *Thalassiosira weissflogii*. Mar. Biol. 142, 949-958.
645 Finkel, Z.V., Beardall, J., Flynn, K.J., Quigg, A., Rees, T.A.V., Raven, J.A. 2010. Phytoplankton
646 in a changing world: Cell size and elemental stoichiometry. J. Plankton Res. 32, 119–137.
647 Flato, G. M. 2005. The third generation coupled global climate model (CGCM3). Environment
648 Canada Canadian Centre for Climate Modelling and Analysis note. Retrieved from
649 http://www.ec.gc.ca/ccmac-cccma/default.asp?n=1299529F-1.

650 Flynn, K.J., Mitra, A. 2009. Building the "perfect beast": Modelling mixotrophic plankton. J.
651 Plankton Res. 31, 965–992.
652 Flynn, K.J., Clark, D.R., Mitra, A., Fabian, H., Hansen, P.J., Glibert, P.M., Wheeler, G.L.,
653 Stoecker, D.K., Blackford, J.C., Brownlee C. 2015. Ocean acidification with
654 (de)eutrophication will alter future phytoplankton growth and succession. Proc. Royal
655 Soc. B, 282, 20142604, doi:10.1098/rspb.2014.2604.
656 Fu, F. X., Tatters, A.O., Hutchins, D.A. 2012. Global change and the future of harmful algal
657 blooms in the ocean. Mar. Ecol. Prog. Ser. 470, 207–233.
658 Glibert, P.M., Magnien, R., Lomas, M.W., Alexander, J., Fan, C., Haramoto, E., Trice, T.M.,
659 Kana, T.M. 2001. Harmful algal blooms in the Chesapeake and Coastal Bays of
660 Maryland, USA: Comparisons of 1997, 1998, and 1999 events. Estuaries 24, 875-883.
661 Glibert, P.M., Seitzinger, S., Heil, C.A., Burkholder, J.M., Parrow, M.W., Codispoti, L.A., Kelly,
662 V. 2005a. The role of eutrophication in the global proliferation of harmful algal blooms:
663 new perspectives and new approaches. Oceanography 18,198-209.
664 Glibert, P.M., Anderson, D.M., Gentien, P., Granéli, E., Sellner, K.G. 2005b. The global,
665 complex phenomena of harmful algal blooms. Oceanography 18, 36-147.
666 Glibert, P.M., Alexander, J., Meritt, D.W., North, E.W., Stoecker, D.K. 2007. Harmful algae
667 pose additional challenges for oyster restoration: Impacts of the harmful algae
668 *Karlodinium veneficum* and *Prorocentrum minimum* on early life stages of the oysters
669 *Crassostrea virginica* and *Crassostrea ariakensis*. J. Shellfish Res. 26, 919-925.
670 Glibert, P.M., Mayorga, E., Seitzinger, S. 2008. *Prorocentrum minimum* tracks anthropogenic
671 nitrogen and phosphorus inputs on a global basis: Application of spatially explicit
672 nutrient export models. Harmful Algae 8, 33-38.

673 Glibert, P.M., Burkholder, J.M., Kana, T.M. 2012. Recent insights about relationships between
674 nutrient availability, forms, and stoichiometry, and the distribution, ecophysiology, and
675 food web effects of pelagic and benthic *Prorocentrum* species. Harmful Algae 14, 231-
676 259.
677 Glibert, P.M., Allen, J.I., Artioli, Y., Beusen, A., Bouwman, L., Harle, J., Holmes, J., Holt, J.
678 2014. Vulnerability of coastal ecosystems to changes in harmful algal bloom distribution
679 in response to climate change: projections based on model analysis. Glob. Chang. Biol.
680 doi: 10.111/gcb.12662.
681 Glibert, P.M., Burford, M.A. 2017. Globally changing nutrient loads and harmful algal blooms:
682 Recent advances, new paradigms and continuing challenges. Oceanography 30(1), 44-55.
683 Glibert, P.M., Burkholder, J.M. 2018. Causes of harmful algal blooms. In: Shumway, S.,
684 Burkholder, J.M., Morton, S.L. (Eds.), Harmful algal blooms: A compendium desk
685 reference. Wiley Blackwell, Singapore, pp. 1-38.
686 Glibert, P.M. 2020. Harmful algal at the complex nexus of eutrophication and climate change.
687 Harmful Algae. doi.org/10.1016/j.hal.2019.03.001.
688 Gómez, F. 2005. A list of free-living dinoflagellate species in the world's oceans. Acta Bot.
689 Croat. 64, 129-212.
690 Gordon, C., Cooper, C., Senior, C.A., Banks, H., Gregory, J.M., Johns, T.C. et al. 2000. The
691 simulation of SST, sea ice extents and ocean heat transports in a version of the Hadley
692 Centre coupled model without flux adjustments. Clim. Dyna. 16(2–3), 147–168.
693 Granéli, E., Edler, L., Gedziorowska, D., Nyman, U. 1985. Influence of humic and fulvic acids
694 on *Prorocentrum minimum* (Pav.) Schiller. In: D.M. Anderson, A.W. White, & D.G.
695 Baden (Eds), Toxic Dinoflagellates (pp. 201-206). Elsevier, New York, New York.

696 Granéli, E., Olsson, P., Sundstrøm, B., Edler, H. 1989. In situ studies of the effects of humic
697 acids on dinoflagellates and diatoms. In: T. Okaichi, D.M. Anderson, and T. Nomoto
698 (Eds.), Red tides: Biology, environmental science and toxicology (pp. 209-212). Elsevier,
699 New York, NY.
700 Grzebyk, D., Berland, B. 1996. Influences of temperature, salinity and irradiance on growth of
701 *Prorocentrum minimum* (Dinophyceae) from the Mediterranean Sea. J. Plankton Res. 18,
702 1837-1849.
703 Gudmundsson, L., Bremnes, J. B., Haugen, J. E. 2012. Technical Note : Downscaling RCM
704 precipitation to the station scale using statistical transformations – a comparison of
705 methods. Hydrol. Earth Syst. Sc. 16, 3383–3390.
706 Haidvogel, D.B., Arango, H., Budgell, W.P., Cornuelle, B.D., Curchitser, E., Di Lorenzo, E., et
707 al. 2008. Ocean forecasting in terrain-following coordinates: formulation and skill
708 assessment of the regional ocean modeling system. J.Comput. Phys. 227(7), 3595-3624.
709 Hall, N.S., Litaker, R.W., Fensin, E., Adolf, J.E., Bowers, H.A., Place, A.R., Paerl, H.W. 2008.
710 Environmental factors contributing to the development and demise of a toxic
711 dinoflagellate (*Karlodinium veneficum*) bloom in a shallow, eutrophic, lagoonal estuary.
712 Estuar. Coasts 31(2), 402-418.
713 Hallegraeff, G.M. 1993. A review of harmful algal blooms and their apparent global increase.
714 Phycologia 32, 79-99.
715 Hallegraeff, G. M. 2010. Ocean climate change, phytoplankton community responses, and
716 harmful algal blooms: a formidable predictive challenge. J. Phycol. 46, 220–235.
717 Harding Jr., L.W., Adolf, J.E., Mallonee, M.E., Miller, W.D., Gallegos, C.L., Perry, E.S.,
718 Johnson, J.M., Sellner, K.G., Paerl, H.W. 2015 Climate effects on phytoplankton floral

composition in Chesapeake Bay. Est. Coast. Shelf Sci. 162, 53-68.

Heil, C.A., Glibert, P.M., Fan, C. 2005. *Prorocentrum minimum* (Pavillard) Schiller: A review of a harmful algal bloom species of growing worldwide importance. Harmful Algae 4, 449-470.

Heil, C.A., Dixon, L.K., Hall, E., Garrett, M., Lenes, J.M., O'Neil, J.M., Walsh, B.M., Bronk, D.A., Killberg-Thoreson, L., Hitchcock, G.L., Meyer, K.A. 2014. Blooms of *Karenia brevis* (Davis) G. Hansen & Ø. Moestrup on the West Florida Shelf: Nutrient sources and potential management strategies based on a multi-year regional study. Harmful Algae 38, 127-140.

Heisler, J., Glibert, P.M., Burkholder, J.M. *et al.* 2008. Eutrophication and harmful algal blooms: A scientific consensus. Harmful Algae 8, 3-13.

Hilton, T.W., Najjar, R. G., Zhong, L., Li, M. 2008. Is there a signal of sea-level rise in Chesapeake Bay salinity? J. Geophys. Res.-Oceans 113: C09002 doi:10.1029/2007JC004247.

Hong, B., Shen, J. 2012. Responses of estuarine salinity and transport processes to potential future sea-level in the Chesapeake Bay. Est., Coast. Shelf Sci. 104-105, 33-45. doi:10.1016/j.ecss.2012.03.014.

Howarth, R.W. 2008. Coastal nitrogen pollution: a review of sources and trends globally and regionally. Harmful Algae 8, 14-20.

Howarth, R.W., Swaney, D.P., Boyer, E.W., Marino, R., Jaworski, N., Goodale, C. 2006. The influence of climate on average nitrogen export from large watersheds in the Northeastern United States. Biogeochemistry 79, 163-186.

741 Irby, I.D., Friedrichs, M. A. M., Friedrichs, C. T., Bever, A. J., Hood, R. R., Lanerolle, L.W.J. ,
742 Scully, M.E., Sellner, K., Shen, J. J. Testa, Li, M., Wang, H., Wang, P., Linker, L., Xia,
743 M. 2016) Challenges associated with modeling low-oxygen waters in Chesapeake Bay: a
744 multiple model comparison. Biogeosciences 13, 2011–2028, doi:10.5194/bg-13-2011-
745 2016.
746 Irby, I.D., Friedrichs, M.A.M., Da, F., Hinson, K.E. 2018. The competing impacts of climate
747 change and nutrient reductions on dissolved oxygen in Chesapeake Bay. Biogeosciences 15,
748 2649–2668.
749 Isleib, R.P.E., Fitzpatrick, J.J., Mueller, J. 2007. The development of a nitrogen control plan for a
750 highly urbanized tidal embayment. Proc.Water Environ. Federation 2007(5), 296-320.
751 Johnson, M. 2014. Inducible mixotrophy in the dinoflagellate *Prorocentrum minimum*. Eukar.
752 Microbiol. 62: 431-443. doi:10.1111/jeu.12198
753 Jones, R., Hassell, D., Hudson, D., Wilson, S., Jenkins, G., Mitchell, J. 2004. Generating high
754 resolution climate change scenarios using PRECIS. Exeter, UK: Met Office Hadley
755 Centre.
756 Lee, S. B., Li, M., Zhang, F. 2017. Impact of sea level rise on tidal range in Chesapeake and
757 Delaware Bays. J. Geophys. Res-Oceans 122(5), 3917-3938.
758 Li, A.S., Stoecker, D.K., Adolf, J.E. 1999. Feeding, pigmentation, photosynthesis and growth of
759 the mixotrophic dinoflagellate *Gyrodinium galatheanum*. Aquat. Microb. Ecol. 19, 163-
760 176.
761 Li, A.S., Stoecker, D.K., Coats, D.W. 2000. Spatial and temporal aspects of *Gyrodinium*
762 *galatheanum* in Chesapeake Bay: distribution and mixotrophy. J. Plankton Res. 22, 2105-
763 24.

764 Li, J., Glibert, P.M., Gao, Y. 2015. Temporal and spatial changes in Chesapeake Bay water
765 quality and relationships to *Prorocentrum minimum*, *Karlodinium veneficum*, and
766 CyanoHAB events, 1991-2008. Harmful Algae 42, 1-14.
767 Li, M., Zhong, L., Boicourt, W.C. 2005. Simulations of Chesapeake Bay estuary : Sensitivity to
768 turbulence mixing parameterizations and comparison with observations. J. Geophys.
769 Res.-Oceans 110, 1–22.
770 Li, M., Zhong, L., Boicourt, W.C., Zhang, S., Zhang. D. 2006. Hurricane-induced storm surges,
771 currents and destratification in a semi-enclosed bay. Geophys. Res. Lett. 33, L02604,
772 doi:10.1029/2005GL024992.
773 Li, M., Lee, Y.J., Testa, J.M., Li, Y., Ni, W., Kemp, W.M., DiToro, D.M. 2016. What drives
774 interannual variability of hypoxia in Chesapeake Bay: Climate forcing versus nutrient
775 loading? Geophys. Res. Lett. 43, 2127–2134.
776 Lin, C.-H., Lyubchich, V., Glibert, P.M. 2018a. Time series models of decadal trends in the
777 harmful algal species *Karlodinium veneficum* in Chesapeake Bay. Harmful Algae 73(C)**,**
778 110-118.
779 Lin, C.-H., Flynn, K.J., Glibert, P.M., Mitra, A. 2018b. Modeling effects of variable nutrient
780 stoichiometry and temperature on mixotrophy in the harmful dinoflagellate *Karlodinium*
781 *veneficum*. Front. Mar. Sci. doi.org/10.3389/fmars.2018.00320.
782 Luckenbach, M.W., Sellner, K.G., Shumway, S.E., Greene, K. 1993. Effects of 2 bloom-forming
783 dinoflagellates, *Prorocentrum minimum* and *Gyrodinium uncatenum*, on the growth and
784 survival of the eastern oyster, *Crassostrea virgi*nica (Gmelin 1791). J. Shellfish Res. 12,
785 411-415.

786 Mearns, L. O., Gutowski, W. J., Jones, R., Leung, R., McGinnis, S., Nunes, A. M. B., et al. 2009.
787 A Regional Climate Change Assessment Program for North America. Eos 90(311).
788 http://doi:10.1029/2009EO360002.
789 Mesinger, F., DiMego, G., Kalnay, E., Mitchell, K., Shafran, P.C., Ebisuzaki, W., et al. 2006.
790 North American Regional Reanalysis. Bull. Am. Meteorol. Soc. 87, 343–360.
791 Miller, W.D. Harding Jr., L.W. 2007. Climate forcing of the spring bloom in Chesapeake Bay,
792 USA. Mar. Ecol. Prog. Ser. 331,11-22.
793 Muller, M.N., Dorantes-Aranda, J.J., Seger, A., Botana, M.T., Brandini, F.P., Hallegraeff, G.M.
794 2019. Ichthyotoxicity of the dinoflagellates *Karlodinium veneficum* in response to
795 changes in seawater pH. Front. Mar. Sci., 6, 82. doi:10.3389/fmars.2019.00082.
796 Najjar, R.G., Pyke, C.R., Adams, M.B., Breitburg, D., Kemp, M., Hershner, C., Howarth, R.,
797 Mulholland, M., Paolisso, M., Secor, D., Sellner, K., Wardrop, D., Wood, R.
798 2010. Potential climate-change impacts on the Chesapeake Bay. Est Coast & Shelf Sci.
799 86, 1–20.
800 Ni, W., Li, M., Ross. A.C., Najjar, R.G. 2019. Large projected decline in dissolved oxygen in a
801 eutrophic estuary due to climate change. J. Geophys. Res-Oceans. doi:
802 10.1029/2019JC015274.
803 Niklitschek, E.J., Secor, D. H.. 2005. Modeling spatial and temporal variation of suitable nursery
804 habitats for Atlantic sturgeon in the Chesapeake Bay. Est. Coast. & Shelf Sci. 64,135–
805 148.
806 O'Neil, J.M., Davis, T.W., Burford, M.A., Gobler, C.A. 2012. The rise of harmful cyanobacteria
807 blooms: the potential roles of eutrophication and climate change. Harmful Algae 14, 313–
808 334.

809 Pal, J.S., Giorgi, F., Bi, X., Elguindi, N., Solmon, F., Gao X., et al. 2007. Regional climate
810 modeling for the developing world: The ICTP RegCM3 and RegCNET. Bull. Am.
811 Meteorol. Soc. 88(9), 1395–1409.
812 Paerl, H.W., Huisman, J. 2008. Blooms like it hot. Science 320, 57-58.
813 Place, A.R., Bowers, H.A., Bachvaroff, T.R., Adolf, J.E., Deeds, J.R., Sheng, J. 2012.
814 *Karlodinium veneficum* —The little dinoflagellate with a big bite. Harmful Algae 14,
815 179-195.
816 Raven, J. A., Ball, L. A., Beardall, J., Giordano, M., Maberly, S.C. 2005. Algae lacking carbon-
817 concentrating mechanisms. Can.J. Bot. 83(7), 879–890.
818 Rost, B., Richter, K.-U., Riebesell, U., Hansen, P.J. 2006. Inorganic carbon acquisition in red
819 tide dinoflagellates. Plant Cell Environ. 29, 810-822.
820 Schaefer, S., Alber, M. 2007. Temperature controls a latitudinal gradient in the proportion of
821 watershed nitrogen exported to coastal ecosystems. Biogeochemistry 85, 333-346.
822 http://doi: 10.1007/s10533-007-9144-9.
823 Schlenger, A.J., North, E.W., Schlag, Z., Li, Y., Secor, D., Smith, K., Niklitschek, E. 2013.
824 Modeling the influence of hypoxia on the potential habitat of Atlantic sturgeon *Acipenser*
825 *oxyrinchus*: A comparison of two methods. Mar. Ecol. Prog. Ser. 483, 257–272.
826 Shchepetkin, A.F., McWilliams, J.C. 2005. The regional oceanic modeling system (ROMS): a
827 split-explicit, free-surface, topography-following-coordinate oceanic model. Ocean
828 model. 9(4), 347-404.
829 Shen, C., Testa, J.M., Li, M., Cai, W-J, Waldbusser, G.G., Ni, W., Kemp, W.M., Cornwall, J.,
830 Chen, B., Brodur, J., Su, J. 2019. Controls on carbonate system dynamics in a coastal

plain estuary: a modelling study. J Geophys. Res.-Biogeosci 124, https://doi.org/10.1029/2018JG004802.

Silva, E.S. 1985. Ecological factors related to Prorocentrum minimum blooms in Obidos Lagoon (Portugal). In. Anderson, D.M., White, A., Baden, D. (Eds.), Toxic dinoflagellates (pp. 251-256). Elsevier, N.Y.

Skamarock, W.C., Klemp, J.B., Dudhia, J., Gill, D. O., Barker, D.M., Wang, W., et al. 2005. A description of the advanced research WRF version 2 (No. NCAR/TN-468+ STR). National Center for Atmospheric Research Boulder Co Mesoscale and Microscale Meteorology Div.

Smayda, T.J. 2002. Turbulence, watermass stratification and harmful algal blooms: an alternative view and frontal zones as "pelagic seed banks." Harmful Algae 1, 95-112.

Smith, K.A., Schlag, Z., North, E.W.. 2018. Estimating habitat volume of living resources using three-dimensional circulation and biogeochemical models. Comput. Geosc. 116, 74-80.

Sommer, U., Paul, C., Moustaka-Gouni, M. 2015. Warming and ocean acidification effects on phytoplankton –from species shifts to size shifts within species in a mesocosm experiment. PLoS ONE 10, e0125239. doi.org/10.1371/journal.pone.0125239.

Stoecker, D.K., Li, A, Coats, D.W., Gustafson, D.E., Nannen, M.K. 1997. Mixotrophy in the dinoflagellate *Prorocentrum minimum*. Mar. Ecol. Prog. Ser. 152: 1-12.

Stoecker, D.K., Adolf, J.E., Place, A.R., Glibert, P.M., Meritt, D. 2008. Effects of the dinoflagellates *Karlodinium veneficum* and *Prorocentrum minimum* on early life history stages of the eastern oyster, *Crassostrea virginica*. Mar. Biol. 154, 81-90.

Stonik, I.V. 1995. A potentially toxic dinoflagellate, *Prorocentrum minimum*, in Amurskii Bay of the Sea of Japan. Russ. J. Mar. Biol. 20, 314-320.

854 Tango, P.J., Magnien, R., Butler, W., Luckett, C., Luckenbach, M., Lacouture, R., Poukish, C.
855 2005. Impacts and potential effects due to *Prorocentrum minimum* blooms in Chesapeake
856 Bay. Harmful Algae 4, 525-531.
857 Testa, J.M., Li, Y., Lee, Y.J., Li, M., Brady, D.C., DiToro, D.M., Kemp, M.K. 2014. Quantifying
858 the effects of nutrient loading on dissolved O 2 cycling and hypoxia in Chesapeake Bay
859 using a coupled hydrodynamic – biogeochemical model. J. Mar. Syst. 139, 139–158.
860 Testa, J.M., Li, Y., Lee, Y.J., Li, M., Brady, D.C., DiToro, D.M., Kemp, W.M. 2017. Modeling
861 physical and biogeochemical controls on dissolved oxygen in Chesapeake Bay: lessons
862 learned from simple and complex approaches. In D. Justic, K. Rose, R. Hetland, and K.
863 Fennel (Eds.) Modeling Coastal Hypoxia - Numerical Simulations of Patterns, Controls
864 and Effects of Dissolved Oxygen Dynamics (pp. 95-118). Springer International
865 Publishing AG, Switzerland.
866 Teutschbein, C., Seibert, J. 2012. Bias correction of regional climate model simulations for
867 hydrological climate-change impact studies: Review and evaluation of different methods.
868 J. Hydrol. 456–457, 12-29.
869 Tyler, M.A., Seliger, H.H. 1978. Annual subsurface transport of a red tide dinoflagellate to its
870 bloom area: water circulation patterns and organism distributions in the Chesapeake Bay.
871 *L*imnol. Oceanogr. 23(2), 227-246.
872 Tyler, M.A., Seliger, H.H. 1981. Selection for a red tide organism: physiological responses to the
873 physical environment. Limnol. Oceanogr. 26(2), 310-324.
874 Wagena, M.B., Collick, A.S., Ross, A., Rau, B., Najjar, R., Sommerlot, A., Fuka, D.R.,
875 Kleinman, P.J., Z.M. Easton. 2018. Quantifying the impact of climate change and climate
876 extremes on hydrologic and biogeochemical processes in the Chesapeake Bay Watershed.

Sci. Total Environ. 637–638, 1443–1454, https://doi.org/10.1016/j.scitotenv.2018.05.116.

Wells, M.L., Trainer, V.L., Smayda, T.J., Karlson, B.S., Trick, C.G., Kudela, R.M., Ishikawa, A., Bernard, S., Wulff, A., Anderson, D.M., Cochlan, W.P. 2015. Harmful algal blooms and climate change: learning from the past and present to forecast the future. Harmful Algae 49, 68-93.

Wikfors, G.H., Smolowitz, R.M. 1995. Experimental and histological studies of 4 life-history stages of the Eastern oyster, *Crassostrea virginica*, exposed to a cultured strain of the dinoflagellate *Prorocentrum minimum*. Biol. Bull. 188, 313-328.

Xie, X., Li, M. 2018. Effects of wind straining on estuarine stratification: A combined observational and modeling Study. J. Geophys. Res.-Oceans 123(4), 2363–2380.

Xie, X., Li, M., Ni, W. 2018. Roles of wind-driven currents and surface waves in sediment resuspension and transport during a tropical storm. J. Geophys. Res.-Oceans, doi: 10.1029/2018JC014104.

Zervas, C. 2009. Sea level variations of the United States 1854-2006. NOAA Technical Report NOS CO-OPS 053.

Zhong, L., Li, M. 2006. Tidal energy fluxes and dissipation in the Chesapeake Bay. Cont. Shelf Res. 26, 752-770.

Figure Captions:

Figure 1. Average cell concentration of *Prorocentrum minimum* (a) and *Karlodinium veneficum* (b) (cell L^{-1}) observed at the monitoring stations in Chesapeake Bay between 2002 and 2011. The size of the symbol represents the range of cell abundance: small black dot < 10^6 cells L^{-1}, open black symbol 1-2 x 10^6 cells L^{-1}, open green symbol 2-10 x 10^6 cells L^{-1}, and open red symbol 10-30 x 10^6 cells L^{-1}. Average fraction of a year when physical conditions produce favorable habitats for *P. minimum* (c) and *K. veneficum* (d). The rivers are marked in (d).

Figure 2. Monthly averaged cell concentration of *Prorocentrum minimum* (a) and *Karlodinium veneficum* (b) at monitoring stations in Chesapeake Bay between 2002 and 2011. The red lines represent the median values, the blue boxes span the interquartile range, and the whiskers are the highest and lowest observations. Monthly averaged fraction of the surface area of Chesapeake Bay where physical conditions are favorable for *P. minimum* (c) and *K. veneficum* (d).

Figure 3. Average fraction of a year when chemical niche (panels a, c) and all criteria (panels b, d) produce favorable habitats for *P. minimum* (panels a,b) and *K. veneficum* (panels c, d).

Figure 4. Monthly averages of (a) river flow, (b) total nitrogen (TN) loading, and (c) total phosphorus (TP) loading from the Susquehanna River.

Figure 5. Average cell concentration of *Prorocentrum minimum* (top row) observed at the monitoring stations in Chesapeake Bay between 2002 and 2011. Symbols for cell ranges as in

Figure 1. Average fraction of a year when physical conditions produce favorable habitats for *P. minimum* (bottom row) for 2002-2011.

Figure 6. Average cell concentration of *Karlodinium veneficum* (top row) observed at the monitoring stations in Chesapeake Bay between 2002 and 2011. Symbols for cell ranges as in Figure 1. Average fraction of a year when physical conditions produce favorable habitats for *K. veneficum* (bottom row) for 2002-2011.

Figure 7. Center of mass of *Prorocentrum minimum* (a)/(b) and *Karlodinium veneficum* (c)/(d) obtained from cell concentration measurements at the monitoring stations (panels a,c) and estimated from the habitat model based on physical criteria (panels b,d). The solid lines in (b) and (d) are the least-square linear regression fit to the habitat model results. In (a) and (c) the dashed lines are the least-square linear regression fits to the cell observations and the solid lines are the linear fits using the same slopes as those in (b) and (d).

Figure 8. Averaged historical Susquehanna River discharge from USGS (a); and projected monthly changes of future Susquehanna River flow by the models WRFG_cgcm3 (b), RCM3_gfdl (c) and HRM3_hadcm3 (d) between past and future. Projected averaged historical surface air temperature (grey line), mean (low-passed, black thick line) and future changes of air temperature (red bar) in the Chesapeake Bay region projected by the same 3 models, WRFG_cgcm3 (e), RCM3_gfdl (f) and HRM3_hadcm3 (g).

941 Figure 9. Changes in the favorable habitat areas for *P. minimum* (a) and *K. veneficum* (b) due to
942 climate change. Results are based on the regional climate model RCM3_gfdl.
943
944 Figure 10. Changes in the favorable habitat seasons for *P. minimum* (panels a-c) and *K.*
945 *veneficum* (panels d-f) due to climate-induced temperature change: RCM3_gfdl (panels a,d);
946 WRFG_cgcm3 (panels b,e); HRM3_hadcm3 (panels c,f).
947
948 Figure 11. Changes in the favorable habitat areas for *P. minimum* due to climate-induced salinity
949 change during peak growing months (April-May): WRFG_cgcm3 (top row); RCM3_gfdl
950 (middle row); HRM3_hadcm3 (bottom row).
951
952 Figure 12. Changes in the favorable habitat areas for *K. veneficum* due to climate-induced
953 salinity change during peak growing months (June-August): WRFG_cgcm3 (top row);
954 RCM3_gfdl (middle row); HRM3_hadcm3 (bottom row).
955
956
957
958 **Table Caption:**
959 Table 1. Rules used in the habitat models for *Prorocentrum minimum* and *Karlodinium*
960 *veneficum*, based on empirical observations of their physical niche and chemical niche.
961

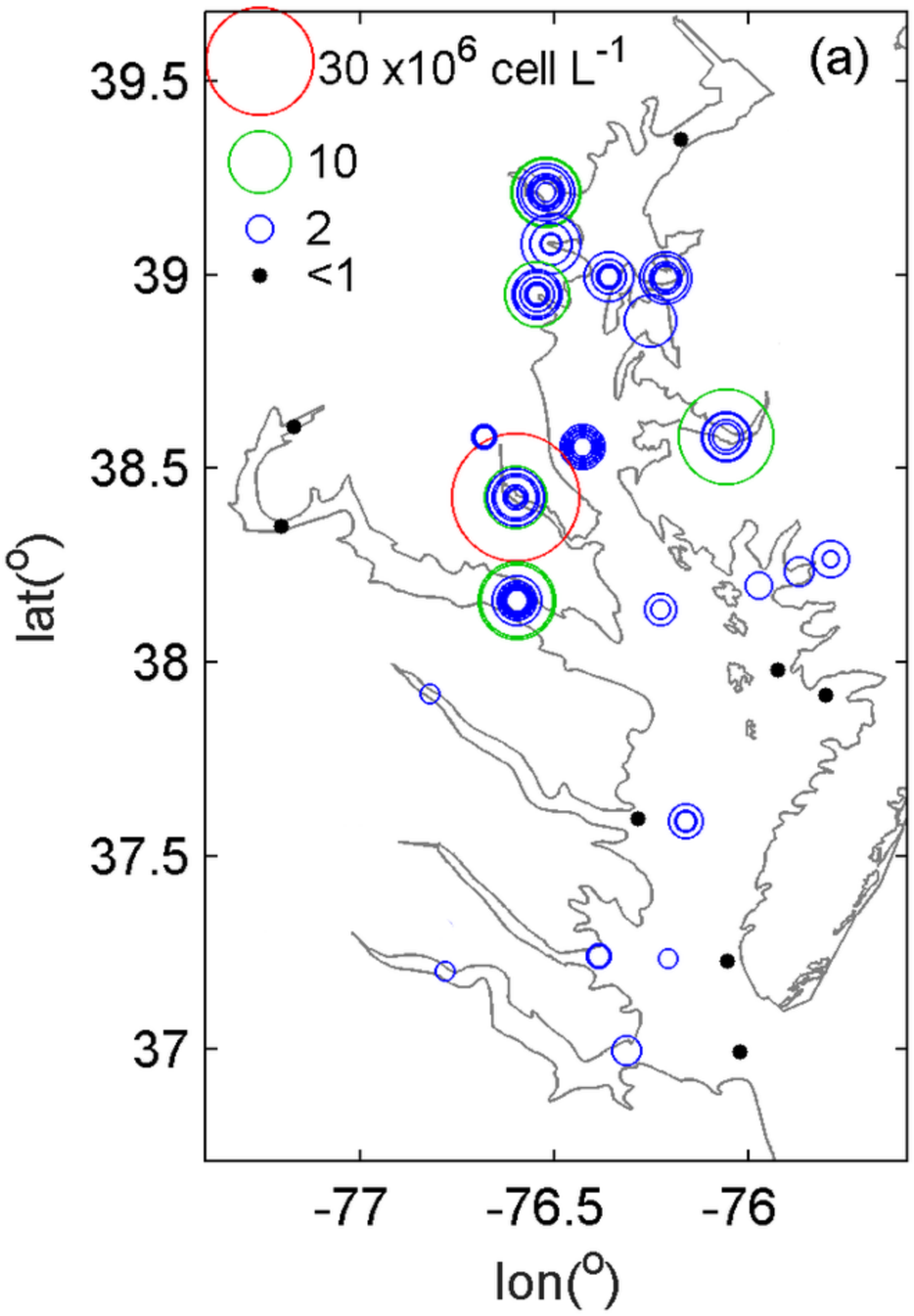
30 x10^6 cell L^-1
10
2
<1
(a)
39.5
39
38.5
38
37.5
37
lat(°)
-77
-76.5
-76
lon(°)

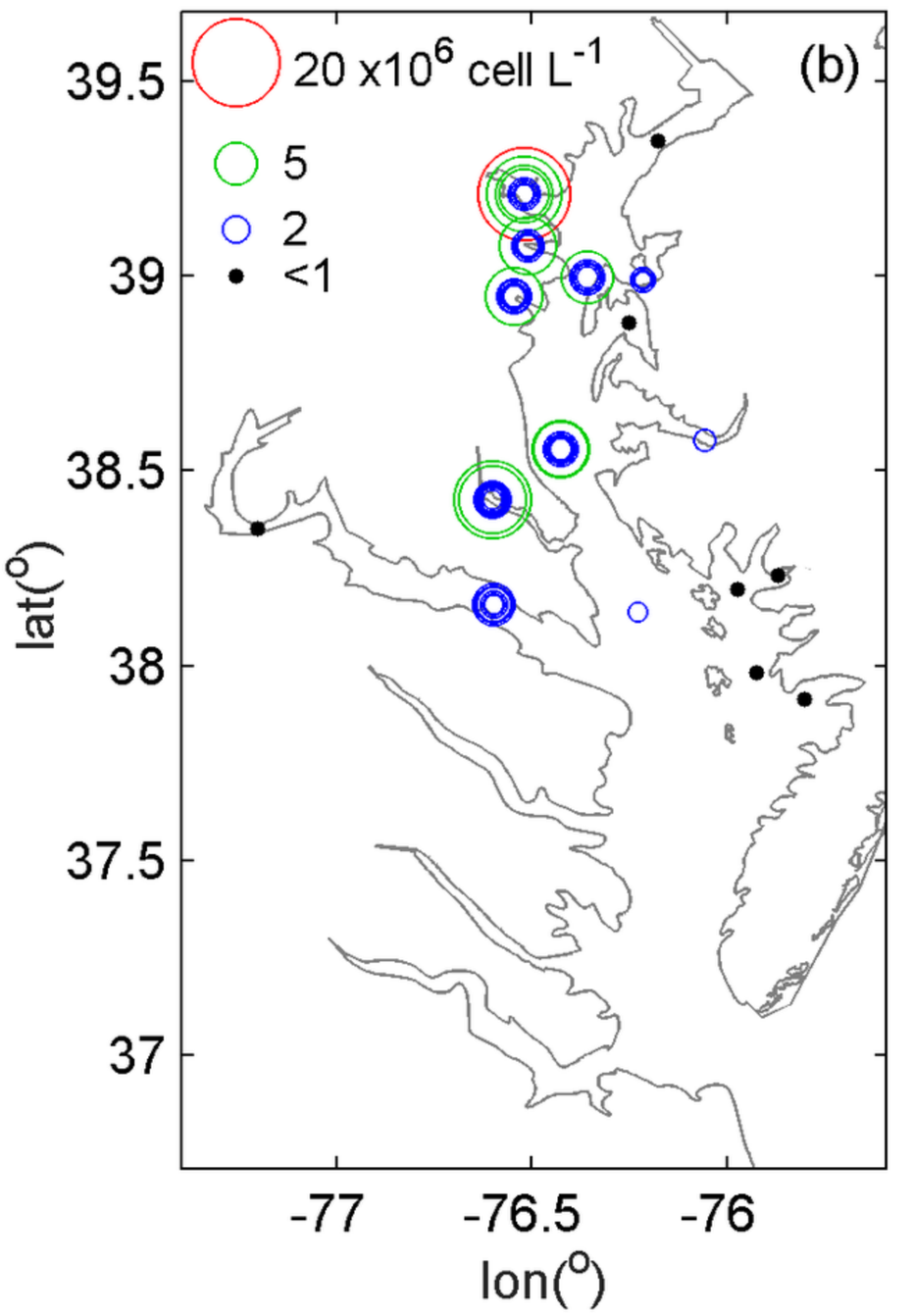
20 x10^6 cell L^-1
5
2
<1
(b)
39.5
39
38.5
38
37.5
37
lat(°)
-77
-76.5
-76
lon(°)

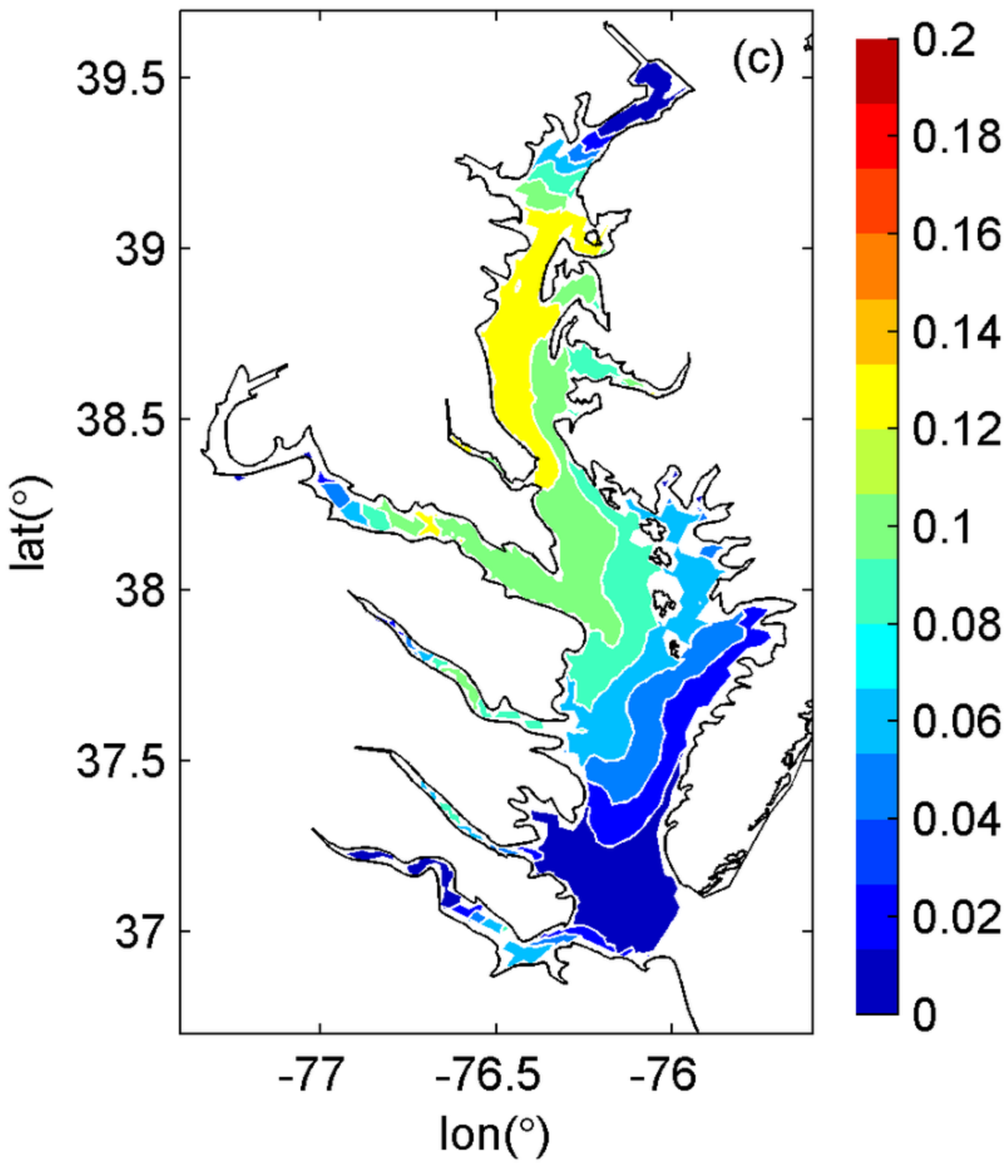
(c)
0.2
0.18
0.16
0.14
0.12
0.1
0.08
0.06
0.04
0.02
0
39.5
39
38.5
38
37.5
37
lat(°)
-77
-76.5
-76
lon(°)

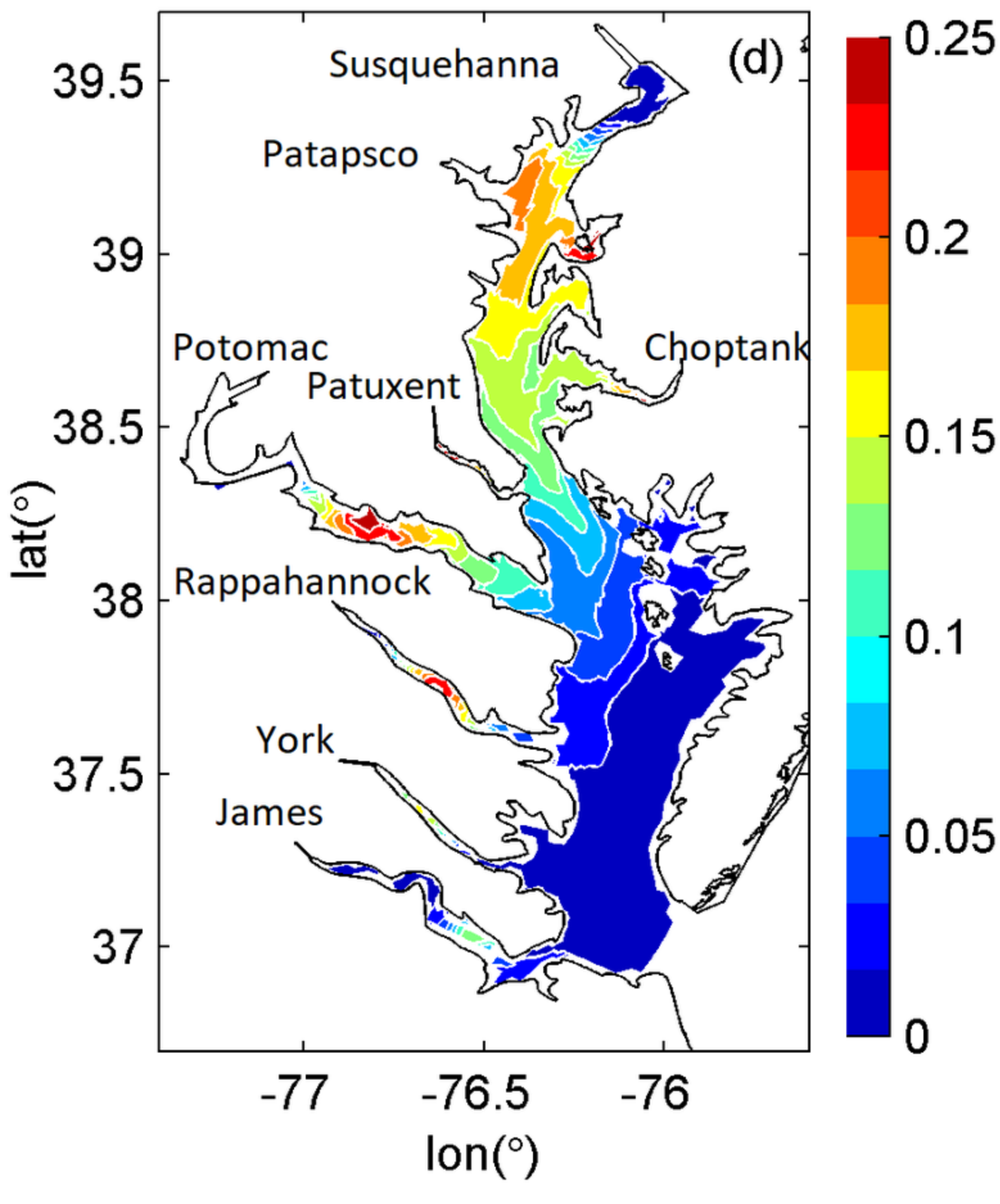
Susquehanna
Patapsco
Potomac
Patuxent
Choptank
Rappahannock
York
James
(d)
0.25
0.2
0.15
0.1
0.05
0
39.5
39
38.5
38
37.5
37
lat(°)
-77
-76.5
-76
lon(°)

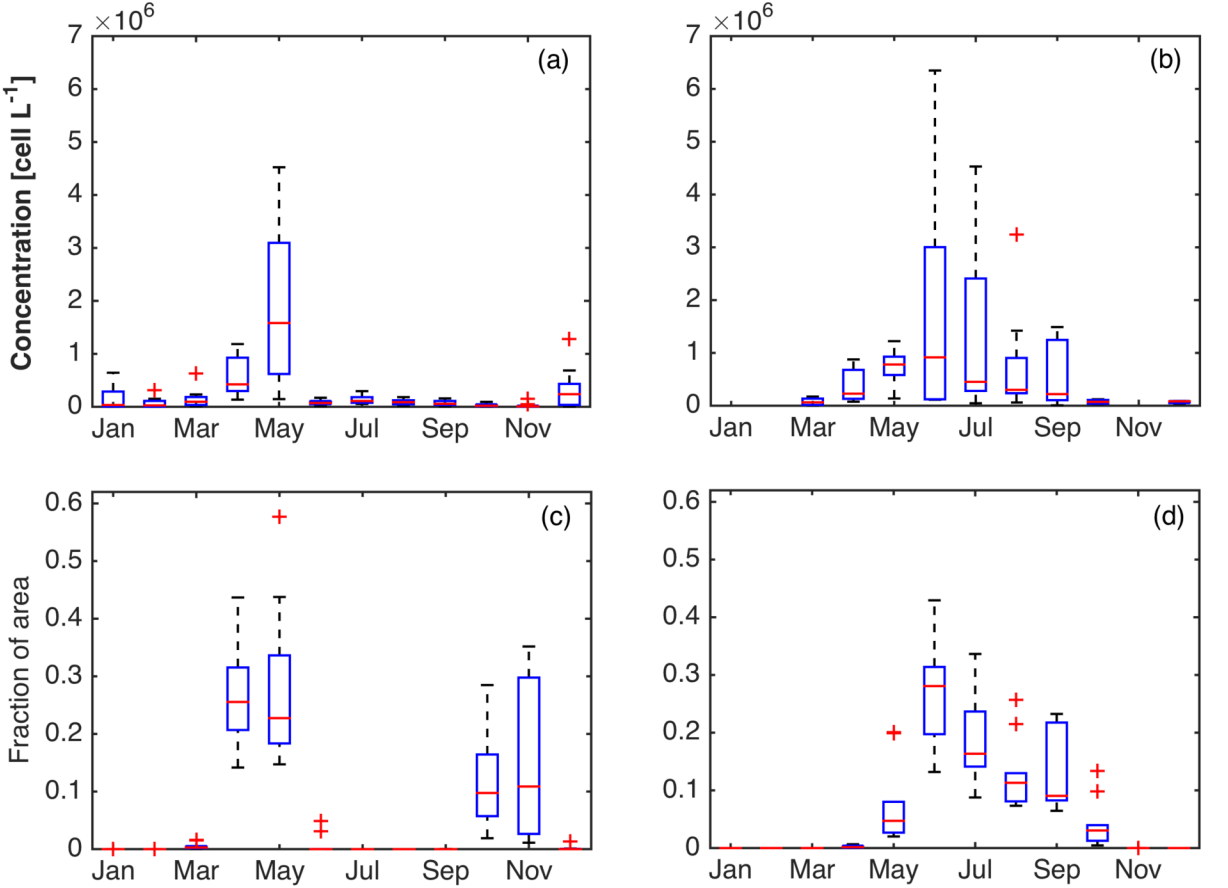
(a)
(b)
(c)
(d)
×10^6
Concentration [cell L^-1]
Fraction of area
Jan
Mar
May
Jul
Sep
Nov
0
1
2
3
4
5
6
7
0.1
0.2
0.3
0.4
0.5
0.6

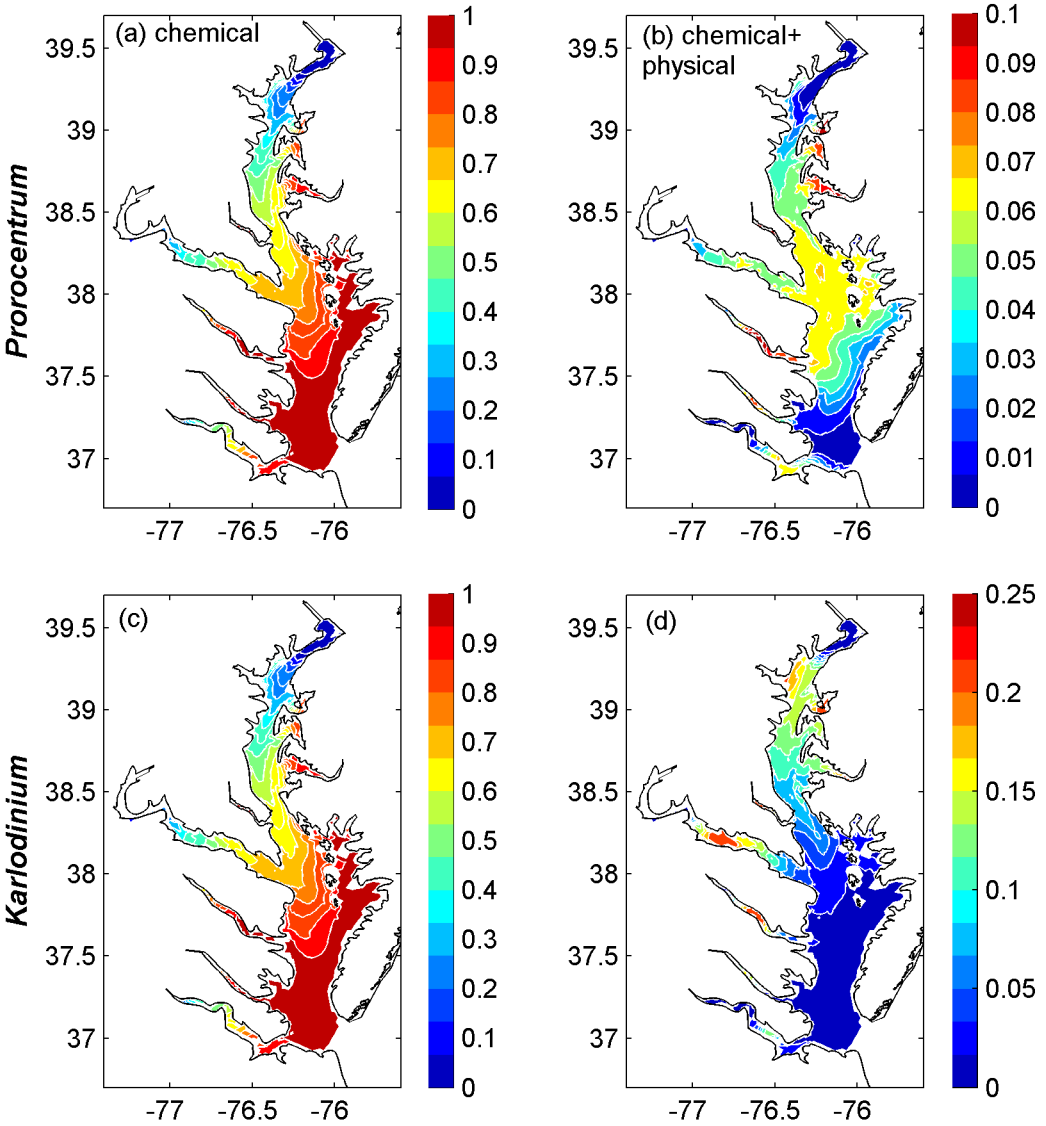
Prorocentrum
Karlodinium
(a) chemical
(b) chemical+ physical
(c)
(d)
39.5
39
38.5
38
37.5
37
-77
-76.5
-76
1
0.9
0.8
0.7
0.6
0.5
0.4
0.3
0.2
0.1
0
0.1
0.09
0.08
0.07
0.06
0.05
0.04
0.03
0.02
0.01
0
0.25
0.2
0.15
0.1
0.05
0

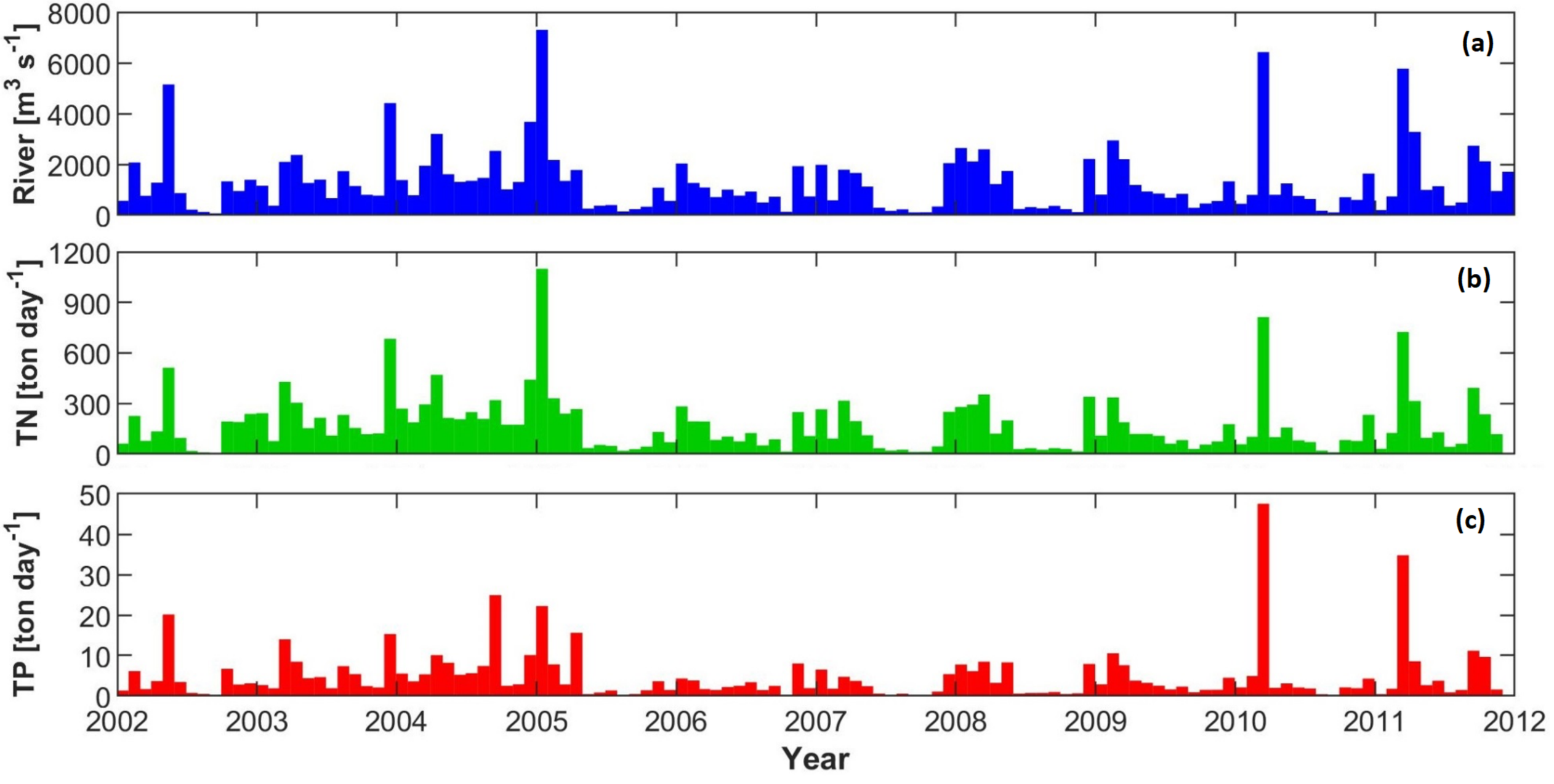
River [m3 s-1]
8000
6000
4000
2000
0
(a)
TN [ton day-1]
1200
900
600
300
0
(b)
TP [ton day-1]
50
40
30
20
10
0
(c)
2002
2003
2004
2005
2006
2007
2008
2009
2010
2011
2012
Year

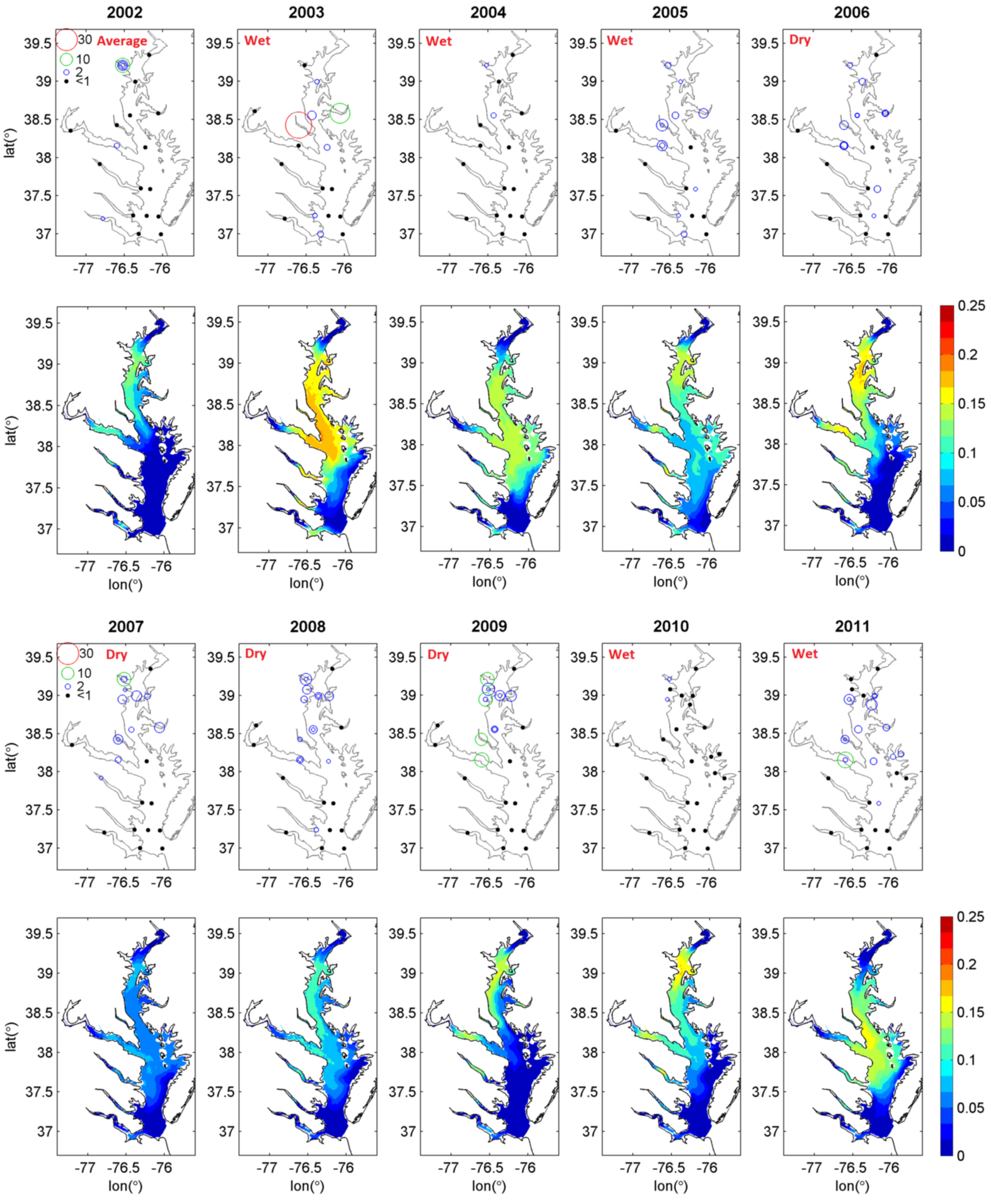
2002
2003
2004
2005
2006
2007
2008
2009
2010
2011
Average
Wet
Wet
Wet
Dry
Dry
Dry
Dry
Wet
Wet
30
10
2
≤1
lat(°)
lon(°)
39.5
39
38.5
38
37.5
37
-77
-76.5
-76
0.25
0.2
0.15
0.1
0.05
0

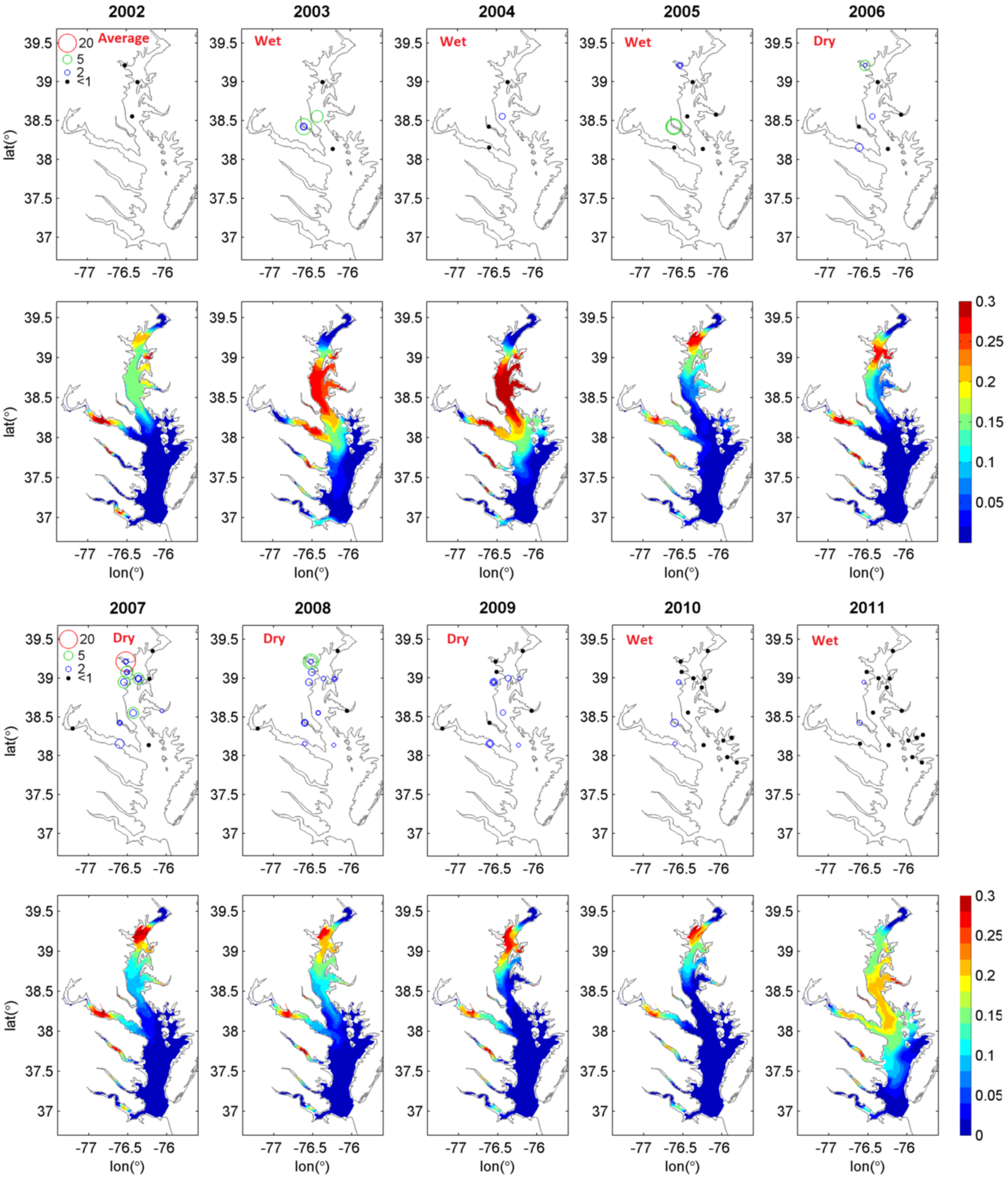
2002
2003
2004
2005
2006
2007
2008
2009
2010
2011
Average
Wet
Wet
Wet
Dry
Dry
Dry
Dry
Wet
Wet
20
5
2
<1
lat(°)
lon(°)
39.5
39
38.5
38
37.5
37
-77
-76.5
-76
0.3
0.25
0.2
0.15
0.1
0.05
0

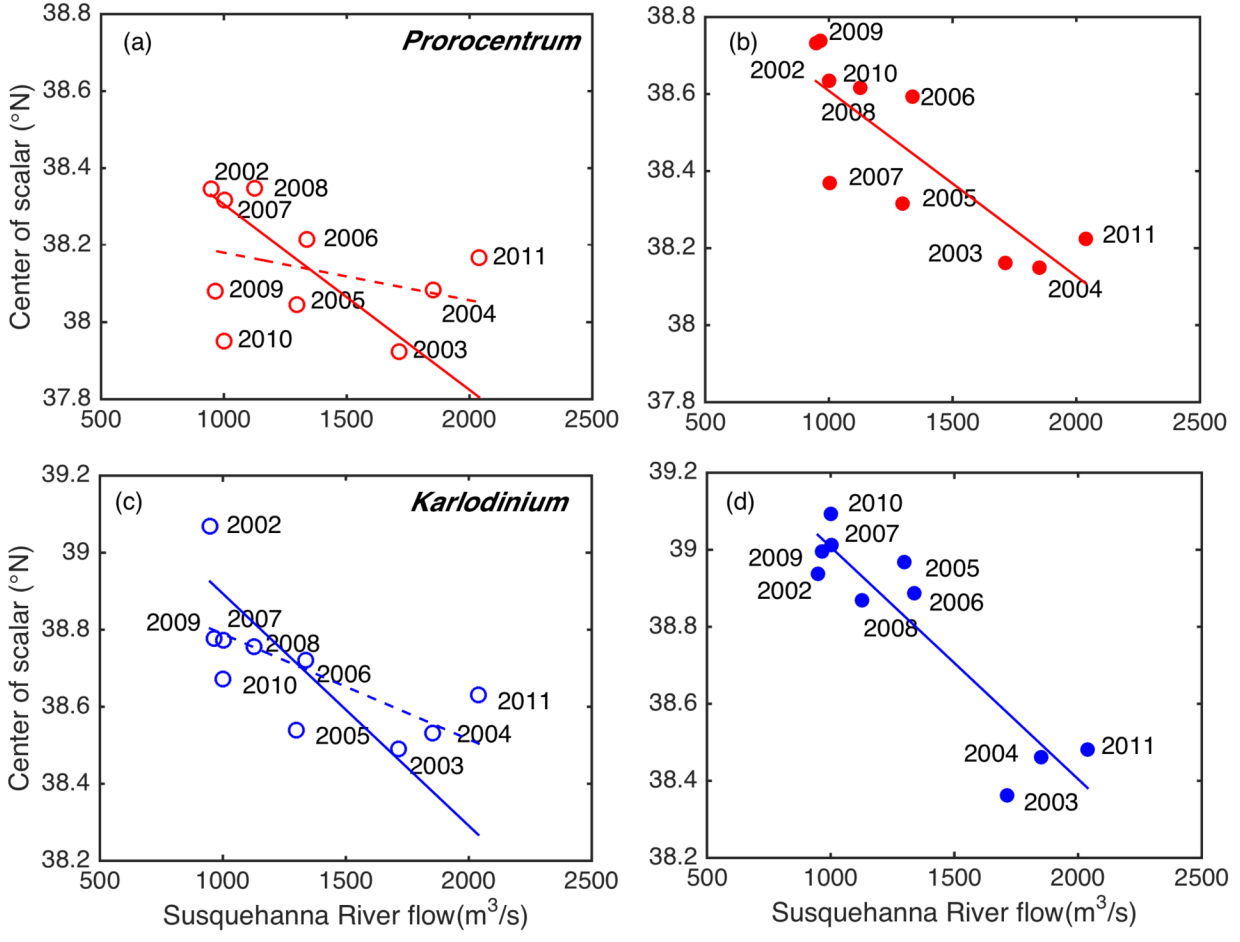
(a)
Prorocentrum
Center of scalar (°N)
2002
2008
2007
2006
2011
2009
2005
2004
2010
2003
(b)
2009
2002
2010
2006
2008
2007
2005
2011
2003
2004
(c)
Karlodinium
2002
2009
2007
2008
2010
2006
2011
2005
2004
2003
Susquehanna River flow(m3/s)
(d)
2010
2007
2009
2005
2002
2006
2008
2004
2011
2003
Susquehanna River flow(m3/s)

River discharge(m^3/s)

4000
2000
0

(a)

Feb Apr Jun Aug Oct Dec

Monthly change (%)

100
50
0
-50

(b)

Feb Apr Jun Aug Oct Dec

100
50
0
-50

(c)

Feb Apr Jun Aug Oct Dec

100
50
0
-50

(d)

Feb Apr Jun Aug Oct Dec

Air temperature(deg C)

30
20
10
0

(e)

Feb Apr Jun Aug Oct Dec

30
20
10
0

(f)

Feb Apr Jun Aug Oct Dec

30
20
10
0

(g)

Feb Apr Jun Aug Oct Dec

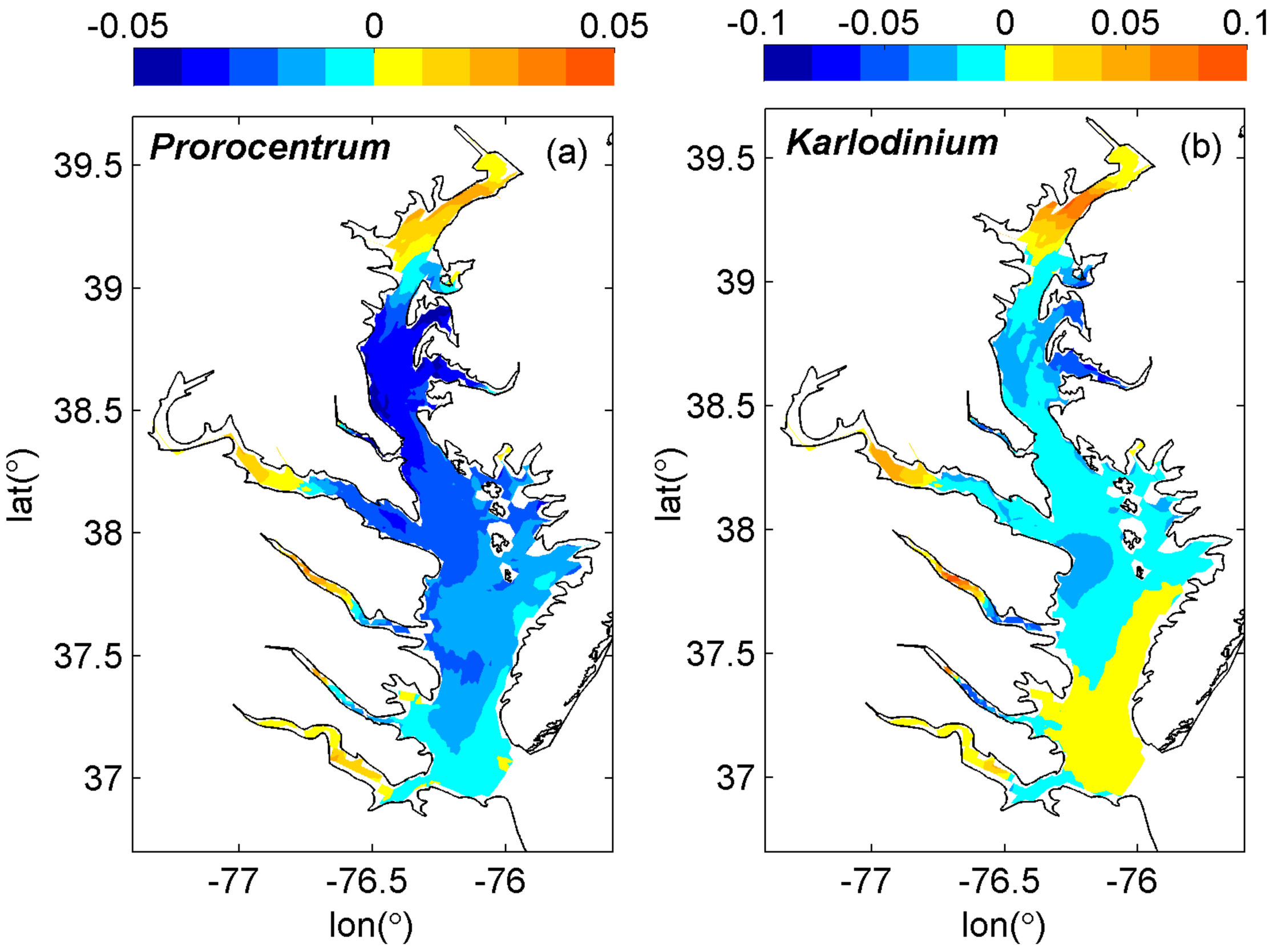
-0.05
0
0.05
Prorocentrum
(a)
39.5
39
38.5
38
37.5
37
lat(°)
-77
-76.5
-76
lon(°)
-0.1
-0.05
0
0.05
0.1
Karlodinium
(b)
39.5
39
38.5
38
37.5
37
lat(°)
-77
-76.5
-76
lon(°)

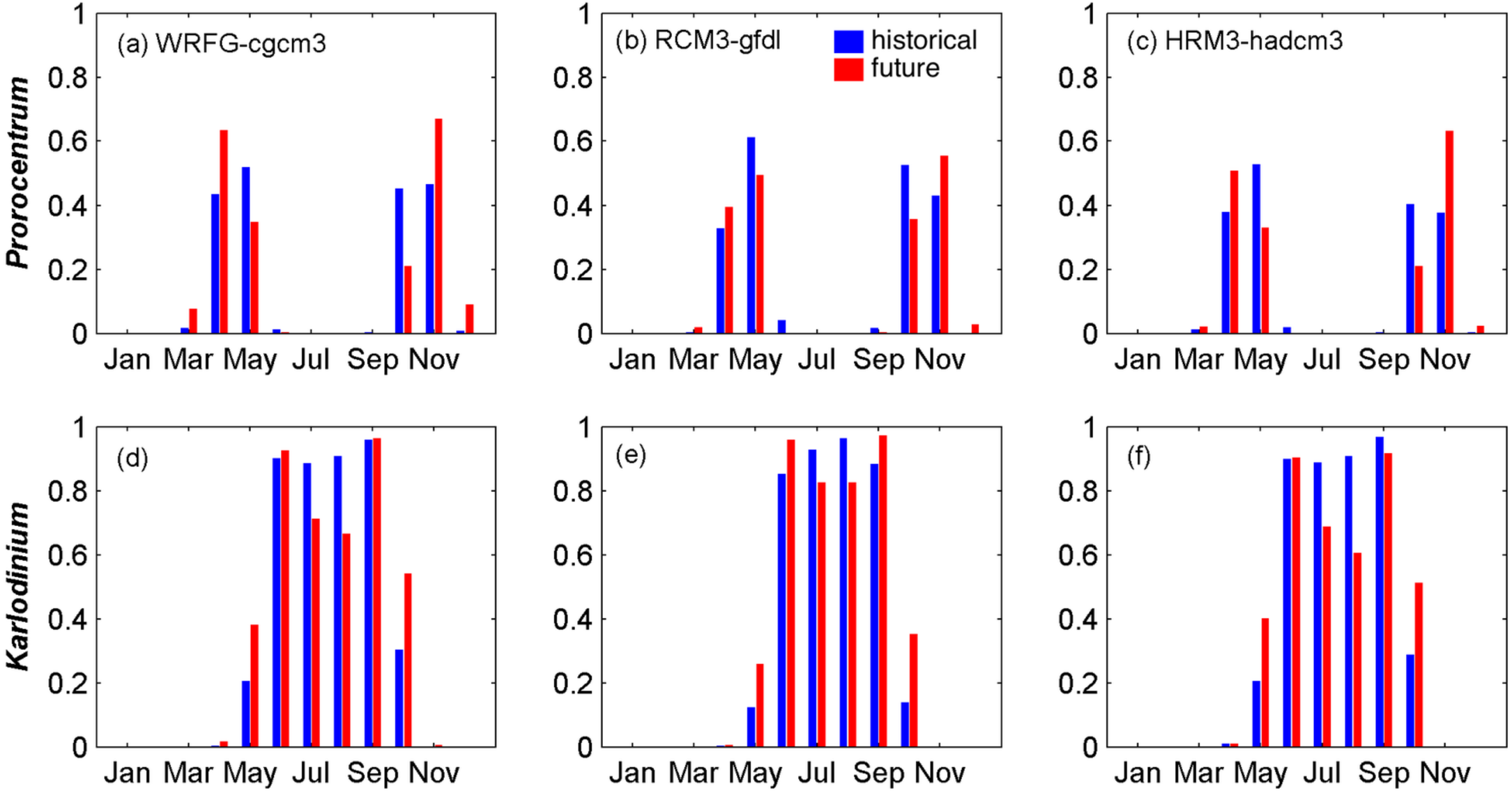
(a) WRFG-cgcm3
(b) RCM3-gfdl
historical
future
(c) HRM3-hadcm3
Prorocentrum
Karlodinium
(d)
(e)
(f)
0
0.2
0.4
0.6
0.8
1
Jan Mar May Jul Sep Nov

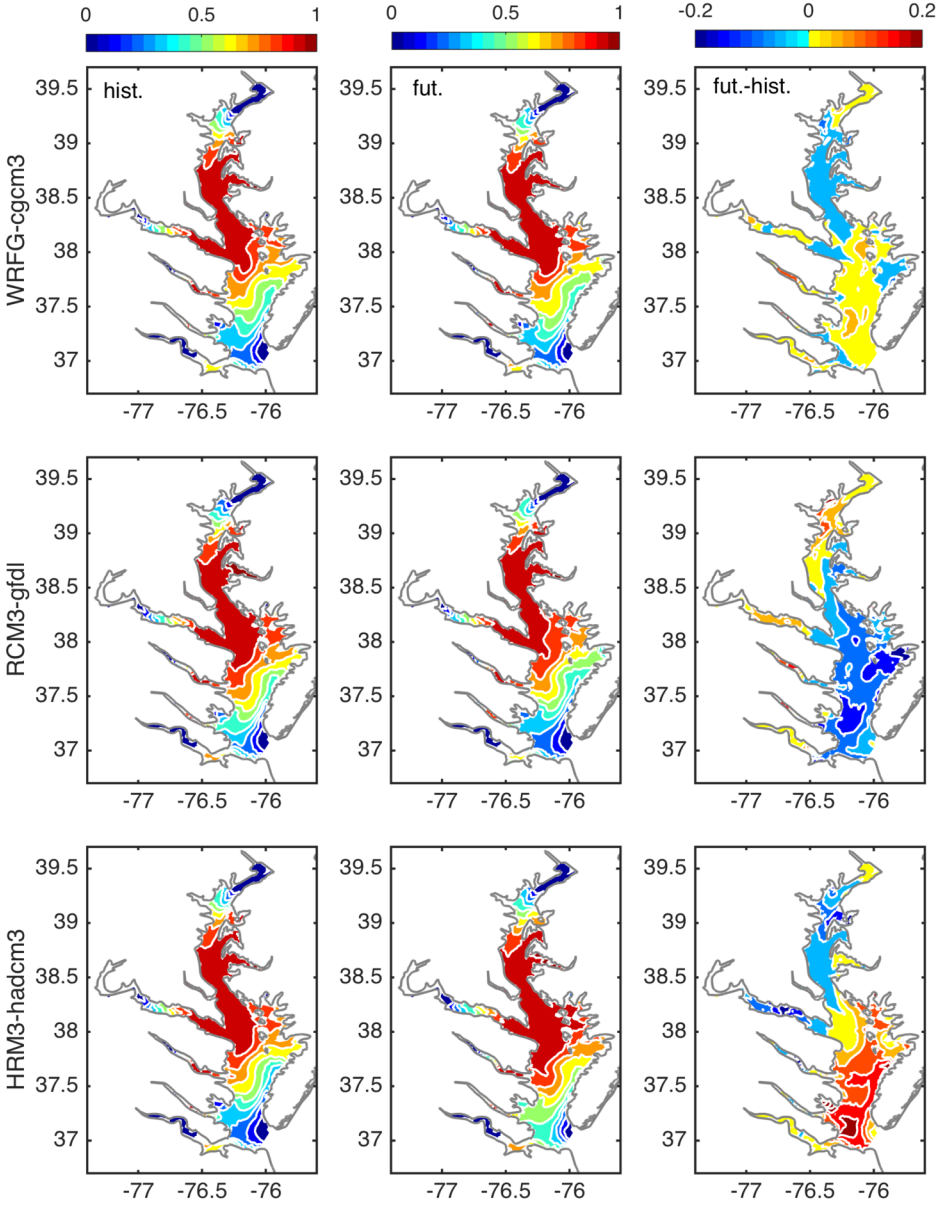
0
0.5
1
0
0.5
1
-0.2
0
0.2
hist.
fut.
fut.-hist.
WRFG-cgcm3
RCM3-gfdl
HRM3-hadcm3
39.5
39
38.5
38
37.5
37
-77
-76.5
-76

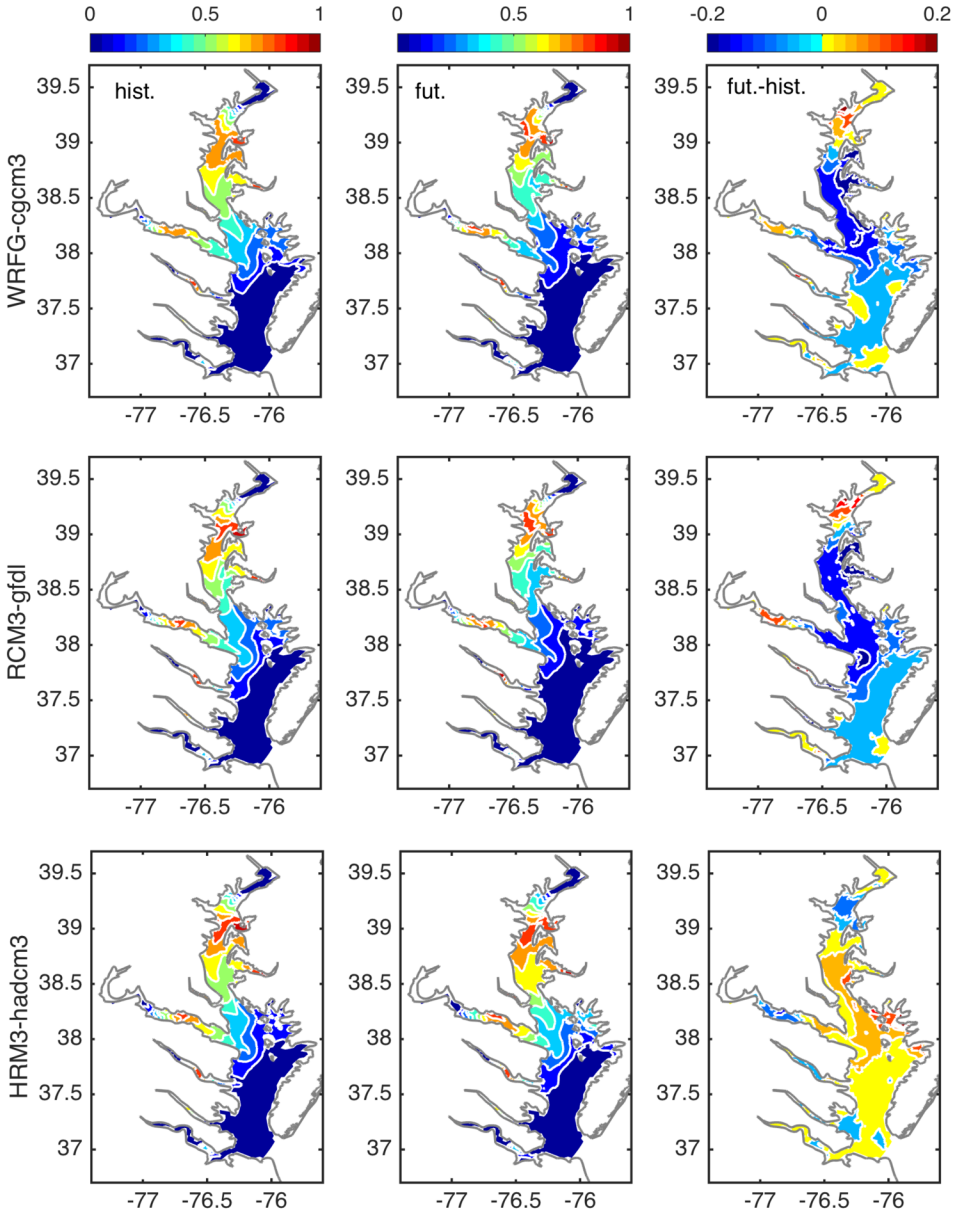
0
0.5
1
0
0.5
1
-0.2
0
0.2
hist.
fut.
fut.-hist.
WRFG-cgcm3
RCM3-gfdl
HRM3-hadcm3
39.5
39
38.5
38
37.5
37
-77
-76.5
-76

		Prorocentrum minimum	*Karlodinium veneficum*
A. Physical niche	Temperature	$13.7<SST<19.1^{o}C$	$21<SST<30^{o}C$
	Salinity	$3<SSS<15$	$5<SSS<12$
B. Chemical niche		$NH_4 > NO_3$	$NH_4 > NO_3$

Prorocentrum

Karlodinium

Abundance

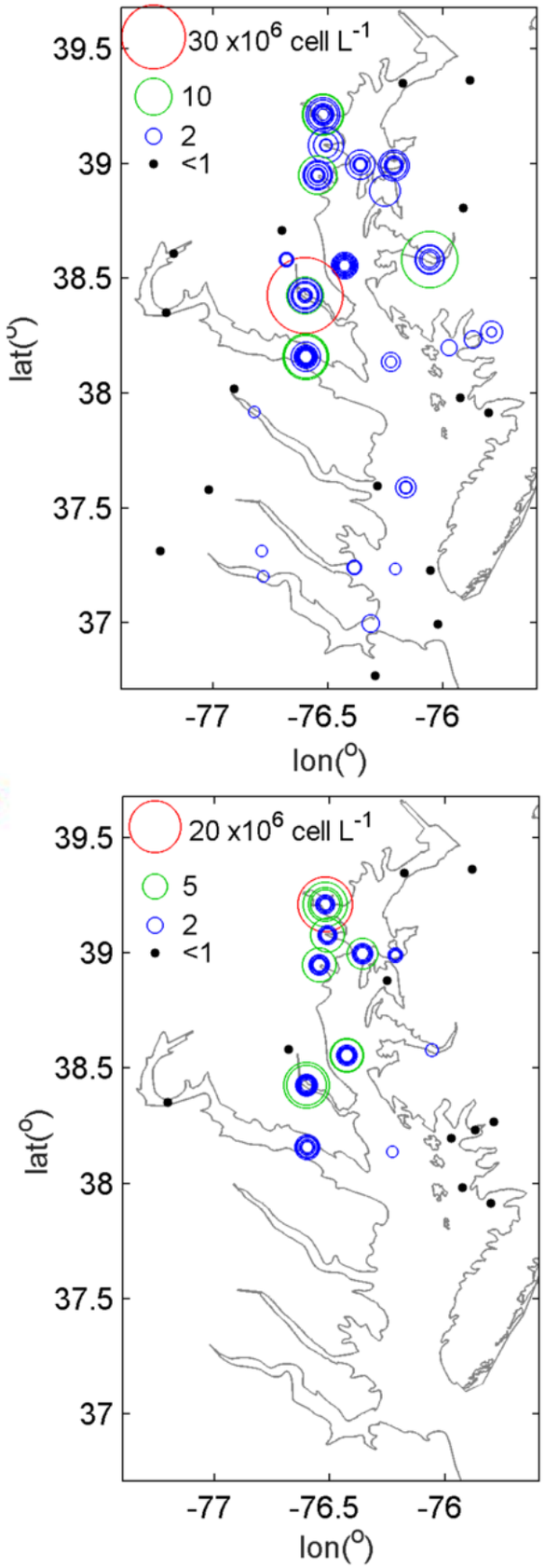

Model-hindcast

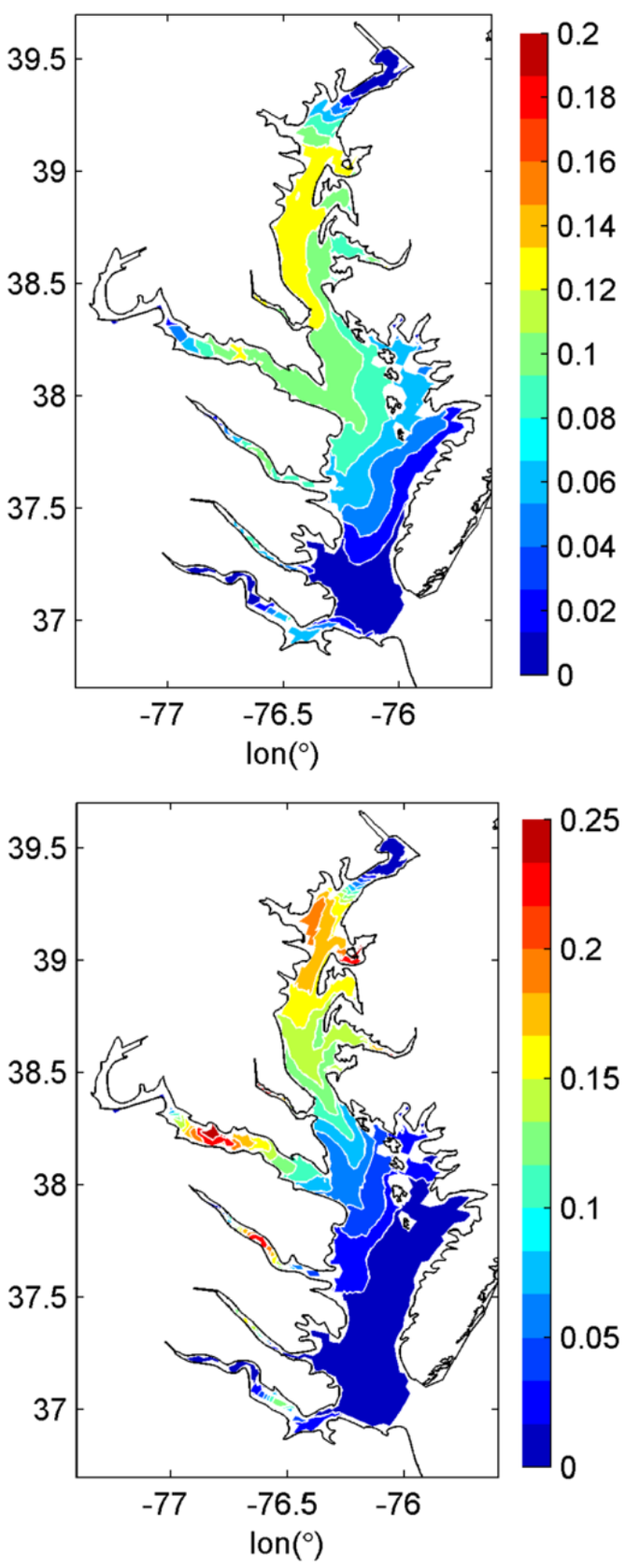

Future-Current